relative to the baseline (the average concentration of four consecutive stable samples defined as 100%).

Western blotting and immunostaining

To determine expression of Piccolo, brain tissue or cell lysate was solubilized in homogenization buffer (150 mM NaCl, 1 mM EDTA, 10 mM Tris, 100 mM Na_2CO_3, pH 11.5) with a mixture of protease inhibitor. After shaking for 30 min and centrifugation at 4 °C, supernatants were subjected to SDS-PAGE (4% polyacrylamide) and transferred to polyvinylidene difluoride membranes. Mouse brains or cultured cells were fixed in 4% paraformaldehyde in PBS and permeabilized with 0.4% Triton X-100.

Cell culture, transfection and [^{3}H]DA uptake

PC12 cells (Riken Bioresource Center Cell Bank, Tsukuba, Japan) were cultured on polyornithine-coated culture coverslips in Dulbecco's modified Eagle's medium (DMEM) supplemented with 10% heat-inactivated horse serum and 5% fetal bovine serum (FBS).[6] For stable expression of hDAT, PC12 cells were transfected with pCMV-hDAT using Lipofectamine 2000 (Invitrogen). A stably transfected pool was selected with 800 μg ml^{-1} geneticin (Invitrogen). For transient expression, the cells were transfected with the plasmids expressing different domain of Piccolo. The primary cultured dopaminergic neurons were separated from ventral midbrains of rat embryos (day 14). [^{3}H]DA uptake in hDAT-PC12 cells was performed as described before.[20] Briefly, cells were washed in Krebs–Ringers–HEPES (KRH) buffer twice before assay. Uptake was initiated by adding 1 μM 3, 4-(ring-2,5,6,-^{3}H)-DA (Perkin Elmer, Waltham, MA) containing 10^{-5} M pargyline and 10^{-5} M ascorbic acid. Uptake proceeded for 10 min at 23 °C and was terminated by three rapid washes in ice-cold KRH buffer. Accumulated [^{3}H]DA was determined by liquid scintillation counting (Beckman LS6500). Nonspecific uptake was defined in the presence of 10 μM GBR12909 (Sigma).

Cell-surface biotinylation and internalization assays

Biotinylation internalization assays were performed as described previously.[6]

Structural models

Molecule models of Piccolo C_2A domain were generated using the amino-acid sequence data from Protein Data Bank (Gi:42543545). The C_2A domain models were energy minimized using Molecular Operating Environment (MOE) software (Chemical Computing Group, Montreal, Canada) to fix any mismatches between the various structural segments. All calculations used an MMFF94x force field and a cutoff distance of 9.5 Å for nonbinding interactions. ASEDock of the MOE program was used for phospholipids and/or Ca^{2+} ions docking stimulation. DSviewer Lite software (Accelry Inc., San Diego, USA) was used for modeling of the electrostatic surface.

Statistics

All data were expressed as means ± s.e.m. Statistical significance was determined by a one-way ANOVA, followed by the Bonferroni–Dunn test for multigroup comparisons. Differences were considered significant when $P<0.05$.

Results

Overexpression of Piccolo in the NAc of METH-treated mice

The reasons for pursuing Piccolo for intensive investigation arose from our preliminary findings in PCR-select cDNA subtraction strategy (Clontech Laboratories, Palo Alto, CA, USA) for detecting the

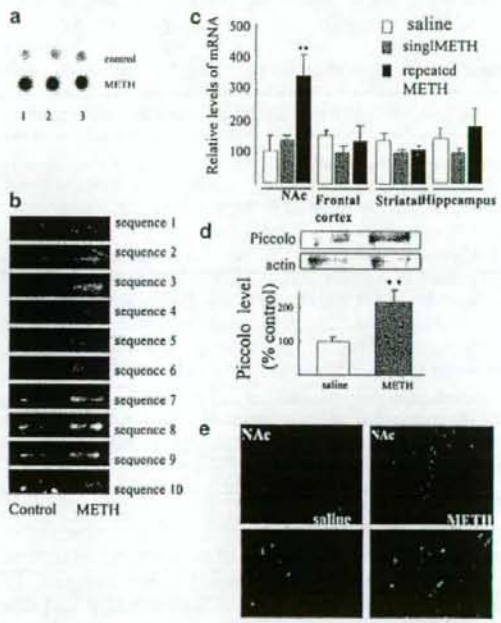

Figure 1 Piccolo expression in nucleus accumbens (NAc) was upregulated by repeated methamphetamine (METH) administration. (**a**) Piccolo overexpression in the NAc of a presentative mouse after daily METH administration for 5 days was shown. (**b**) RT–PCR analysis revealed a significant increase in the productions of the target sequences of Piccolo induced by METH. (**c**) Piccolo mRNA production was elevated significantly in NAc, rather than in the frontal cortex, striatal and hippocampus, of the mice treated with repeated METH. Data are expressed as percent of mRNA level of NAc in saline-treated mice ($n=6$). $^{**}P<0.01$, compared with saline or single dosing of METH (in NAc). (**d**) Western blotting analysis showed the elevation of Piccolo level in NAc responding to repeated METH. $^{**}P<0.01$, compared with saline. (**e**) Immunostaining showed the elevation of Piccolo immunoreactivity in the NAc of the mice administrated with repeated METH. Saline-treated mice (left column) and METH-treated mice (right column).

affected genes in the NAc by METH. The C57BL/6J mice were daily administrated with METH (2 mg kg^{-1}, s.c.) for 5 days, and Piccolo mRNA production in the NAc was found to increase by 240% in comparison to that of saline-treated mice (Figure 1a). Although little is known about the function of Piccolo in drug-induced behavioral sensitization, its subcellular localization, molecular functions and interacting partners led us to presume that Piccolo overexpression elicited by METH could be involved in DA signaling strength and presynaptic plasticity.

We performed a series of experiments to validate the results from PCR-select cDNA subtraction. After the mice were daily administrated with METH (1 mg kg^{-1}, s.c.) for 5 days, Piccolo mRNA levels in the NAc were measured semiquantitatively by RT–PCR. As Piccolo possesses several splicing domain structures, we amplified and analyzed 10 different target sequences. As shown in Figure 1b, repeated METH administration significantly elevated the mRNA productions of the target sequences of Piccolo in NAc. To confirm such alterations, the mRNA productions of Piccolo in different brain regions were measured quantitatively by real-time RT–PCR 2 h after single METH dosing (1 mg kg^{-1}, s.c.) or the final injection of daily METH administration (1 mg kg^{-1}, s.c.) for 5 days. As shown in Figure 1c, the levels of Piccolo mRNA in the frontal cortex, striatal or hippocampus were not affected by either single or repeated METH administration. Remarkably, Piccolo mRNA level in the NAc was increased following repeated METH administration ($F_{(2,15)} = 5.58$; $P < 0.05$), whereas it was not altered by single METH injection. We then examined Piccolo expression in the NAc using western blotting. Consistently, Piccolo protein level in NAc was elevated apparently after repeated METH administration ($t_{(1,8)} = 7.35$; $P < 0.01$; Figure 1d). Immunostaining also revealed a strengthened Piccolo immunoreactivity in NAc of the mice treated with repeated METH (Figure 1e). Taken together, our data suggest a selective increase of Piccolo expression in NAc of behaviorally sensitized mice induced by repeated METH dosing, rather than a global increase of the brain. Because NAc is a brain area closely associated with drug dependence, we presumed that Piccolo overexpression may be involved in dopaminergic plasticity in neural circuits, which is critical for reward.

Piccolo modulates behavioral plasticity and synaptic DA concentration in NAc

To correlate Piccolo expression with the behavioral and neurochemical phenotype to METH, we utilized an AS strategy, which has been widely used to manipulate gene expressions in the brain via intracerebroventricular infusion.[21] The designed AS, which directs against nucleotides 2452–2466, has been demonstrated to downregulate successfully the expression of Piccolo in previous studies.[17] Additionally, a SC was used as a control.

The mice were infused continuously with AS, SC or CSF using implanted osmotic minipumps for 3 days before daily saline or METH administration (1 mg kg^{-1}, s.c.) for 5 days. Such infusion was sustained till the end of each behavioral test. Locomotor activities of mice were measured at days 1, 3 and 5 immediately after drug injection (Figure 2a). There was no difference among Piccolo AS-, SC- or CSF-treated mice in baseline locomotor activity throughout a 30 min habituation period (data not shown) or in response to saline (Figure 2b). Repeated METH administration caused a progressive hyperlocomotion in mice, and interestingly, AS-pretreated mice developed a greater hyperlocomotor activity than those treated with SC or CSF after METH administration for 3 days ($F_{(2,15)} = 5.47$; $P < 0.05$; Figure 2c). Furthermore, such enhanced hyperlocomotor activity was sustained till day 5 despite that the difference was not significant compared with that of SC- or CSF-pretreated mice.

We then investigated the potential role of Piccolo in the rewarding effects by the CPP, a classical conditioning paradigm in which animals learn to prefer an environment associated with drug exposure. The mice were infused with AS, SC or CSF for 3 days before the training of CPP (Figure 2d). As shown in Figure 2e, the CSF-treated mice showed baseline preference for either side of the test chambers prior to METH administration, and developed the significant place conditioning after training with METH ($F_{(5,42)} = 9.12$; $P < 0.05$). Notably, the Piccolo AS-pretreated mice showed approximately a double degree of place conditioning compared to those treated with SC or CSF, indicating that the AS-treated mice developed an enhancement of rewarding effect to METH. The mice were killed immediately after the behavioral test to measure Piccolo protein levels in NAc. Piccolo expression in NAc responding to METH was dramatically increased, whereas AS effectively decreased its expression (Figure 2f). These results indicate that Piccolo downregulation was sufficient to confer METH-enhanced sensitization and rewarding effect, which is mediated predominantly by the dopaminergic system. No evidence of neurotoxicity in pathological histology was found outside of the mechanical disruption produced by implantation of the infusion cannula in our experimental conditions (data not shown).

We finally measured DA release in the NAc by a microdialysis technique. The mice were infused with Piccolo AS, SC or CSF for 3 days before daily METH administration (1 mg kg^{-1}, s.c.) for 3 days (Figure 2g). The basal levels of DA in NAc did not differ among CSF-, AS- or SC-treated mice (CSF, 0.58 ± 0.21 nM; AS, 0.49 ± 0.17 nM; SC, 0.60 ± 0.18 nM) before the final challenge of METH. As expected, DA levels in the NAc were markedly increased immediately after the final challenge of METH. Obviously, AS pretreatment promoted METH-induced DA release in the NAc compared with SC or CSF ($F_{(2,9)} = 5.874$; $P < 0.05$; Figure 2h). These data strongly supported

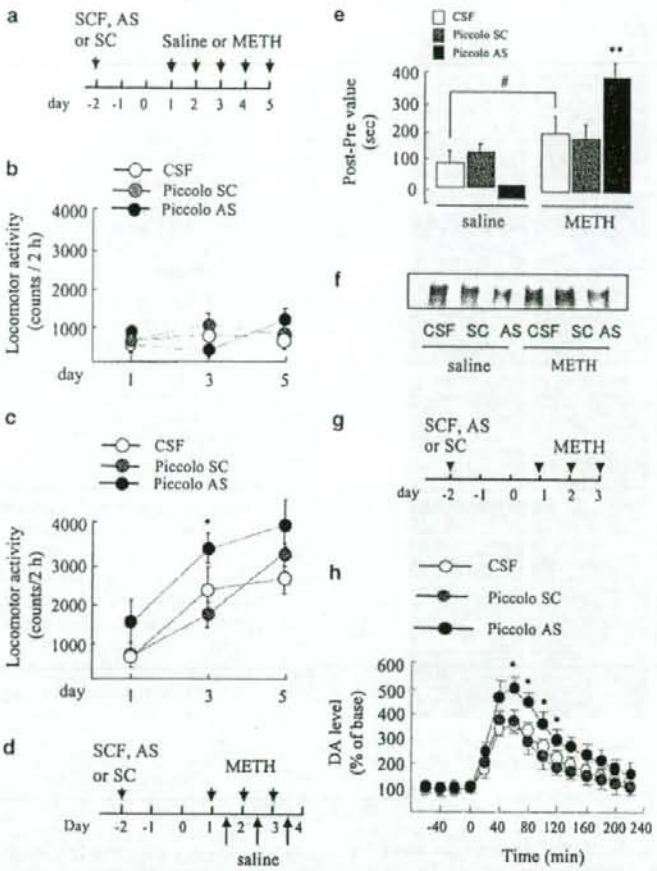

Figure 2 Downregulation of Piccolo expression with antisense oligodeoxynucleotide (AS) promoted methamphetamine (METH)-induced behavioral and synaptic plasticity. (**a–c**) Mice were infused intracerebroventricularly with Piccolo AS, scramble oligodeoxynucleotide (SC) or cerebrospinal fluid (CSF) for 3 days before daily saline (b) or METH (c) administration for 5 days. Locomotor activities were measured at days 1, 3 and 5 ($n = 6$). $^{*}P < 0.05$, compared with SC or CSF. (**d**, **e**) Mice were infused with Piccolo AS, SC or CSF for 3 days before conditioned place-preference (CPP) training. On day 4, the post-conditioning test was performed ($n = 8$). $^{**}P < 0.01$, compared with SC or CSF in METH-treated groups, $^{*}P < 0.05$, compared with CSF in saline-treated group. (**f**) The presentative immunoblots from western blotting indicated that Piccolo expression in the nucleus accumbens (NAc) was inhibited by AS in the mice treated by repeated METH. (**g**, **h**) Mice were infused with AS, SC or CSF for 3 days, followed by daily METH administration for 3 days. Microdialysis was conducted after the final METH injection ($n = 4$). $^{*}P < 0.05$, compared with SC or CSF at the same time point.

the findings in behavioral tests, suggesting that the enhanced accumulation of DA in NAc resulted from AS may contribute to the amplified responsiveness to METH; moreover, Piccolo may play a role in modulating synaptic DA concentration. Taken these results together, Piccolo overexpression in NAc may present a mechanism of opposing the behavioral responsiveness to METH.

Piccolo is colocalized in dopaminergic neurons

To study whether Piccolo is expressed in dopaminergic neurons, double immunostaining was performed in primary cultured dopaminergic neurons. The immunoreactivities of Piccolo and TH revealed an extensive overlap along neuronal projections, indicating that Piccolo is present at dopaminergic synapse (Figure 3a). Notably, abundant Piccolo immunoreactivity was observed as clusters and puncta at the dopaminergic terminals (Figure 3b). Moreover, we also found that almost all of the DAT-immunopositive clusters were present at Piccolo-containing clusters situated along dendritic profiles (Figure 3c), implying the potential interplay of these two molecules. These results strongly support the conclusion that Piccolo is a shared component of the dopaminergic synapses.

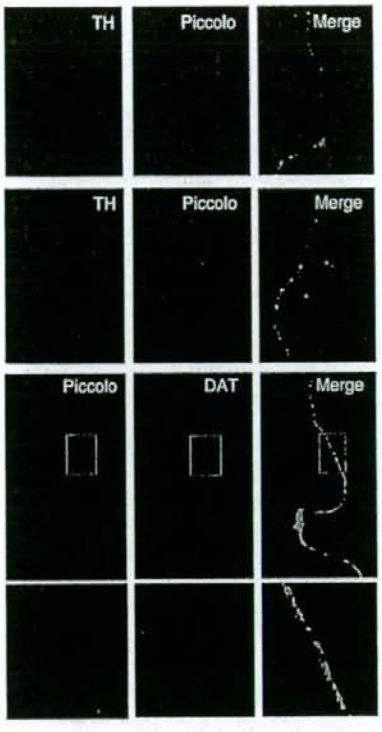

Figure 3 Expression of Piccolo in dopaminergic neurons. (a) Double immunostaining showed that Piccolo is expressed in tyrosine hydroxylase (TH)-positive neurons. (b) Abundant expression of Piccolo is present at the presynaptic component of cultured dopaminergic neurons. (c) Dopamine transporter (DAT) immunoreactivity along the dendritic profiles is paralleled with that of Piccolo.

Piccolo C_2A domain attenuates the inhibition of DA uptake induced by METH through modulating plasmalemmal DAT expression

Total DAT expression levels showed no changes when hDAT-PC12 cells were exposed to either METH (1 μM) for various time periods or concentrations for 30 min (Figures 4a and b). However, the level of cell surface hDAT was reduced in time-dependent manner, and importantly, such reduction was paralleled with the extent of the inhibition of [^{3}H]DA uptake ($F_{(4,15)} = 25.6$, $P < 0.001$; Figure 4c). Similar results were also obtained in dose-dependent studies, which showed a good correlation of the level of surface hDAT and [^{3}H]DA uptake responding to various concentrations of METH ($F_{(4,15)} = 73.0$, $P < 0.001$; Figure 4d).

The schematic representations of C_2A domain, PDZ domain and a fragment between C_2A domain and PDZ domain are shown in Figure 4e. The C_2A domain, PDZ domain or the fragment were expressed in hDAT-PC12 cells to investigate the changes in [^{3}H]DA uptake. We found that the cells transfected with C_2A domain showed a slight, but not significant, increase in [^{3}H]DA uptake in response to saline; moreover, transfection of PDZ domain or p13192 did not alter [^{3}H]DA uptake, either (Figure 4f, left panel). We then pretreated the cells with 1 μM METH for 30 min, followed by [^{3}H]DA uptake assay. METH obviously inhibited [^{3}H]DA uptake, and importantly, C_2A domain-transfected cells showed a higher level of [^{3}H]DA uptake compared with empty pCMV (Stratagene, La Jolla, CA; $F_{(3,20)} = 18.68$, $P < 0.01$), indicating that the C_2A domain expression could attenuate METH-induced inhibition of DA uptake (Figure 4f, right panel).

Because an increase in DA uptake could be resulted from more DAT molecules expressed at the cell surface, we introduced these vectors into hDAT-PC12 cells, and analyzed plasmalemmal hDAT expression by cell-surface biotinylation. The expression levels of cell-surface hDAT did not increase significantly after transfection of C_2A domain, PDZ domain or p13192 in basal conditions (Figure 4g). When the cells were pretreated with 1 μM METH for 30 min, C_2A domain transfection significantly attenuated the decrease in cell surface hDAT level compared to pCMV ($F_{(3,8)} = 14.61$, $P < 0.01$), whereas PDZ domain and p13192 showed no effects (Figure 4h). Such change was consistent with that of [^{3}H]DA uptake shown in Figure 4f, indicating that Piccolo C_2A domain may attenuate the METH-induced inhibition of DA uptake and maintain DAT expression at cell surface.

Piccolo C_2A domain modulates DAT internalization by a mechanism of membrane association

Given that DAT can be internalized and/or recycled, we speculated that the decreased lose of membrane DAT induced by METH in C_2A domain-transfected cells could be resulted from attenuated DAT internalization. To test this hypothesis, DAT internalization was measured by reversible biotinylation in hDAT-PC12 cells. We found that C_2A domain expression could not affect the basal DAT internalization, as revealed by the similar amount of internalized DAT among all groups (Figure 5a). However, DAT internalization was significantly attenuated by C_2A domain expression when the cells were exposed to 1 μM METH for 30 min ($F_{(3,8)} = 8.55$, $P < 0.01$; Figure 5b). Expression of both PDZ domain and p13192 failed to affect the basal or METH-induced DAT internalization. Double immunostaining for hDAT and c-Myc-tagged C_2A domain showed the similar findings that the cells transfected with C_2A domain still maintained a strong plasmalemmal hDAT immunoreactivity responding to METH, whereas a relatively large amount of internalized hDAT was observed in cytosolic compartments of the cells transfected with empty pCMV (Figure 5c). These results indicated that Piccolo C_2A domain attenuates METH-induced DAT internalization, which accounts for the decrease in the loss of DAT at cell surface.

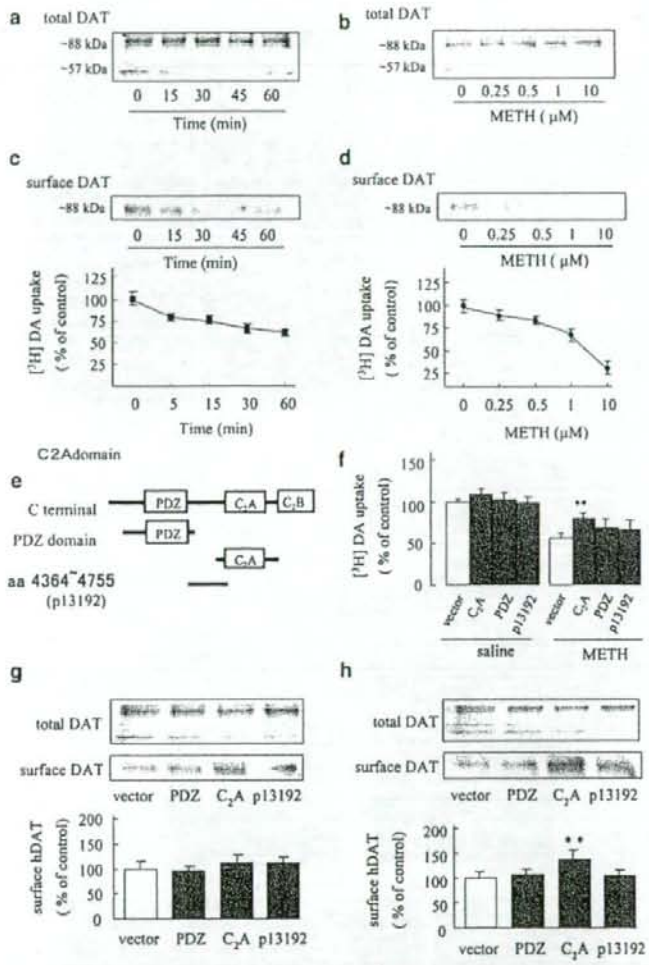

Figure 4 Piccolo C_2A domain increased dopamine (DA) uptake and dopamine transporter (DAT) surface expression. (**a**, **b**) Methamphetamine (METH) could not alter the total DAT expression levels in hDAT-PC12 cells in both time- (**a**) and dose-dependent studies (**b**). (**c**) METH (1 μM) decreased plasmalemmal DAT expression (top) in time-dependent manner, which was paralleled with the decrease in [^{3}H]DA uptake (bottom). $^{**}P<0.01$, compared with the basal level. (**d**) METH decreased DAT expression at the cell surface dose-dependently (top), which was consistent with the decrease in [^{3}H]DA uptake (bottom). $^{**}P<0.01$ and $^{*}P<0.05$, compared with the basal level. (**e**) Schematic representations of C_2A domain, PDZ domain and a fragment (amino acid 4364–4755). (**f**) Piccolo C_2A domain attenuated the METH-induced inhibition of [^{3}H]DA uptake (right panel), but failed to change the basal DA uptake (left panel) ($n=6$). $^{**}P<0.01$, compared with pCMV. (**g**, **h**) Piccolo C_2A domain could not influence DAT surface expression in hDAT-PC12 cells responding to saline (**g**). However, it attenuated METH-induced loss of surface DAT (h). $^{**}P<0.01$, compared with pCMV in METH-treated group.

To study the potential mechanism underlying the action of Piccolo C_2A domain on DAT internalization, we introduced C_2A domain into hDAT-PC12 cells and then analyzed membrane subcellular distributions of Piccolo, C_2A domain, hDAT as well as PIP_2. The cells were homogenized in regular RIPA buffer containing 1% Triton-X 100, and separated into a soluble supernatant and a particulate membrane fraction (120 000 g, 60-min pellet). The latter was solubilized again in RIPA buffer or RIPA buffer containing 0.1 M Na_2CO_3 (pH 11.5), which can extract a major part of detergent-resistant Piccolo protein from brain tissues.[12] As shown in Figure 5d, Piccolo, Piccolo C_2A domain and PIP_2 did not fractionate like a soluble cytosolic protein but was mainly found in membrane sediment extracted by Na_2CO_3, indicating that a substantial

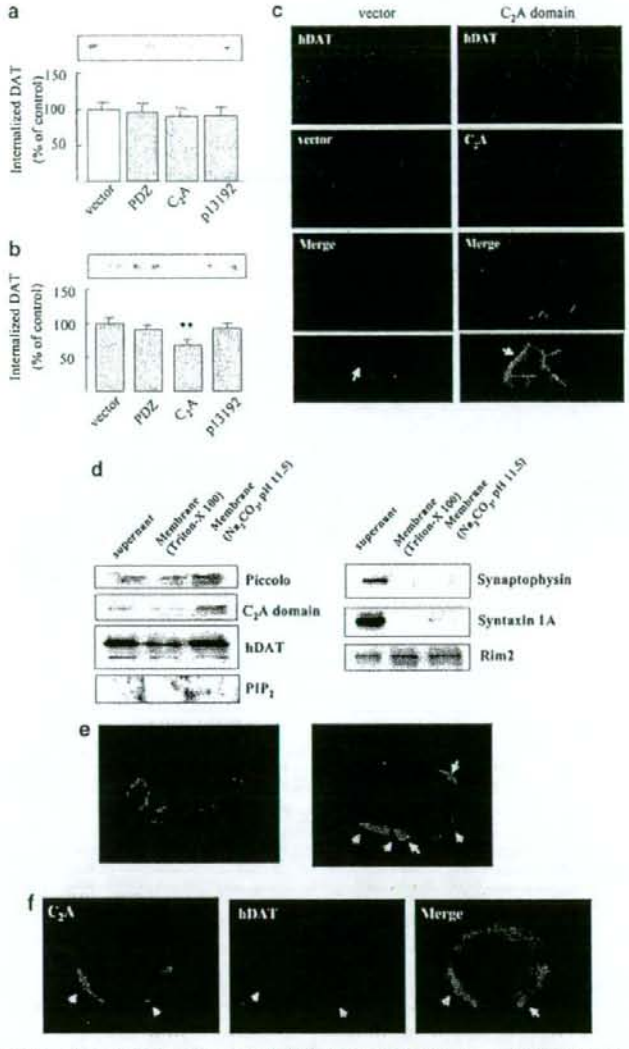

Figure 5 Piccolo modulates dopamine transporter (DAT) internalization by a mechanism of membrane association. (**a, b**) After transfection with various vectors the hDAT-PC12 cells were biotinylated and treated with either saline (**a**) or 1 μM methamphetamine (METH) (**b**) for 30 min to initiate endocytosis. Top, representative blots of internalized hDAT. Bottom, quantitation of hDAT immunoreactivity. $P<0.01$, compared with empty vector (pCMV) in METH-treated group. (**c**) The internalization of hDAT (red) was triggered by exposure of 1 μM METH for 30 min. The cells transfected with empty vector (pCMV) show enriched internalized hDAT (left panel), whereas the cells transfected with c-Myc-tagged-C_2A domain (green) reveal the strong plasmalemmal hDAT immunoreactivity (right panel). Internalized hDAT is depicted. (**d**) Distributions of Piccolo, c-Myc-tagged C_2A domain, hDAT, PIP_2 and other presynaptic proteins in hDAT-PC12 cells. The cells and membrane fractions were extracted with RIPA buffer containing 0.1 M Na_2CO_3 (pH 11.5) or not. (**e**) The transfected Piccolo C_2A domain specially targets plasma membrane in hDAT-PC12 cells. (**f**) Piccolo C_2A domain shows a paralleled immunoreactivity pattern at plasmalemmal rafts with hDAT (arrowhead).

fraction of membrane-bound Piccolo, C_2A domain and PIP_2 are associated with the same plasmalemmal rafts. Interestingly, a significant amount of hDAT was also recovered in both soluble fraction and membrane sediment extracted by Na_2CO_3, indicating that a relatively major part of membrane DAT is localized at the same subcellular fraction with Piccolo C_2A domain and PIP_2. The similar distributions of these

components in lipid raft fractions hint that C_2A domain–PIP_2 interaction may be involved in the distribution of plasmalemmal DAT. In contrast, syntaxin 1A and synaptophysin, the integral membrane proteins, were almost completely recovered in soluble cytosolic fraction, but not in a detergent-resistant fraction. Rim 2, a scaffolding protein with C_2 domain, is known to interact with Piccolo and to regulate presynaptic events. However, its similar subdistribution in the three fractions was different from that of Piccolo C_2A domain. To get an insight into the interplay among DAT, Piccolo C_2A domain and PIP_2, double immunostaining was performed. We found that Piccolo C_2A domain mainly anchored nonuniformly to the inner leaflet of plasma membrane (Figure 5e), which is consistent with its property of targeting membrane PIP_2. Notably, the distribution pattern of C_2A domain resembled that of hDAT, as revealed by the paralleled immunoreactivities at membrane microdomains (Figure 5f).

Internalization of plasmalemmal DAT is PIP_2-dependent

The concept of PIP_2 as a spatially localized regulator of membrane trafficking is clearly illustrated by its key role in clathrin-mediated endocytosis for transporter. If plasmalemmal DAT is triggered to internalize by METH, it should be accompanied by PIP_2 for recruiting endocytic adaptors through PIP_2-binding modules. To test this idea, hDAT and PIP_2 were double-stained in hDAT-PC12 cells after treatment of saline or 1 μM METH for 30 min. Surprisingly, the internalized DAT triggered by METH was found to colocalize with the PIP_2 in the cytosolic compartment (Figure 6, bottom panel), whereas the saline-treated cells only showed the constitutively internalized PIP_2 and DAT (Figure 6, top panel). These results further demonstrated that DAT internalization is also a clathrin-dependent process requiring the assembly of endocytic components like PIP_2.

Interaction of Piccolo C_2A domain and PIP_2

Although Piccolo C_2A domain binding to PIP_2 has been demonstrated using artificial membranes,[15] there is no evidence indicating interaction of the two molecules in living models. We first investigated whether plasmalemmal clusters of Piccolo immunoreactivity coincide with sites of local PIP_2 accumulation using double immunostaining. The clusters of Piccolo immunoreactivities in dendrite profile colocalized precisely with those of PIP_2 in the primary cultured dopaminergic neurons (Figure 7a). Moreover, the localization of transfected C_2A domain in hDAT-PC12 cells was similar with that of PIP_2, which revealed a patchy staining pattern at plasma membrane (Figure 7b). Importantly, the clusters with strong immunoreactivity of C_2A domain also showed substantially larger and stronger labeling macroscopic of PIP_2 clusters, indicating that C_2A domain may sequester PIP_2, thus augmenting the formation of microscopically detectable plasmalemmal PIP_2 clusters.

To better understand the interaction of the two molecules, we generated a PIs binding model of Piccolo C_2A domain with Ca^{2+} docking. As show in Figure 7c, the three-dimensional structure indicated that the predicted PIs binding sites are Ca^{2+}-binding loops at the top of C_2A domain, which shows the similar binding residues for phosphatidylinositol (PI), phosphatidylinositol 4-phosphate (PIP) and PIP_2. Notably, the crystal packing contacts for PIP_2 were the clusters of basic/aromatic residues including 4668–4670 (DNN), 4697–4698 (QK), 4738–4743 (DYDRFS) and 4746 (D). The potential importance of these residues is highlighted by the fact that they are completely conserved among rat, mouse, human and chicken Piccolo.[22] Calculation of the electrostatic surface potential of C_2A domain showed that PIP_2 binding sites are positively charged (Figure 7d), further indicating that clustering PIs by C_2A domain depends on electrostatic interactions between the

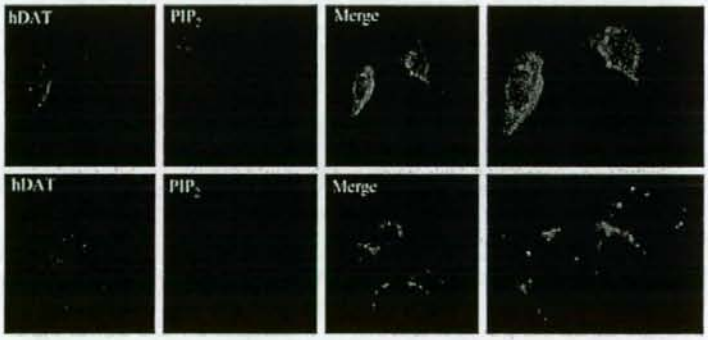

Figure 6 Piccolo C_2A domain attenuates dopamine transporter (DAT) internalization responding to methamphetamine (METH). Double-immunostaining of PIP_2 (red) and hDAT (green) in hDAT-PC12 cells. The internalization of hDAT was promoted by METH, which is accompanied by PIP_2 (bottom panel). The saline-treated cells show strong immunoreactivities of both hDAT and PIP_2 (top panel).

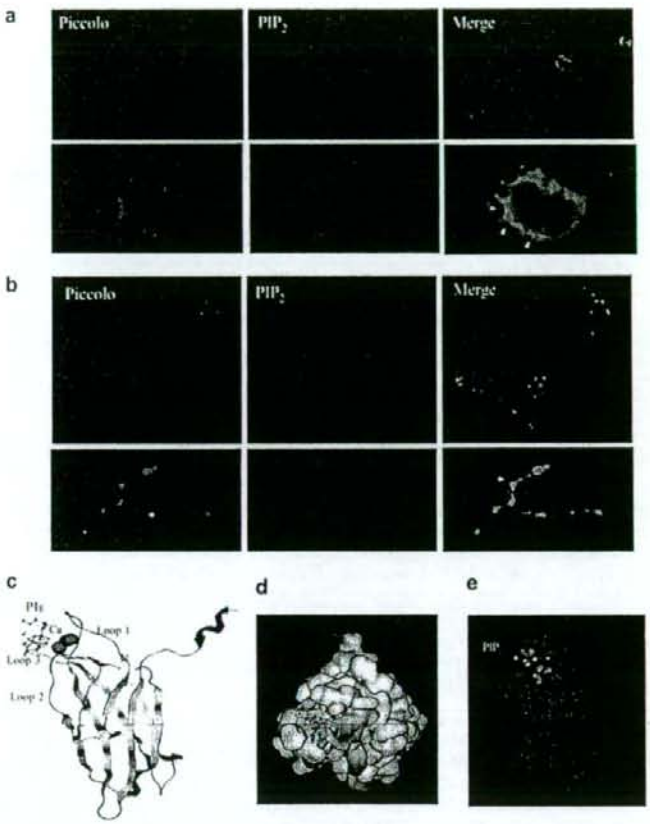

Figure 7 Interaction of Piccolo and PIP_2. (**a**) PIP_2 (red) colocalizes precisely with Piccolo (green) along the presynaptic terminal in primary cultured dopaminergic neurons (arrowed). (**b**) PIP_2 (red) accumulates at plasmalemmal rafts, where it colocalizes with Piccolo (green) in hDAT-PC12 cells. Arrowheads point to regions of intense staining of PIP_2 and Piccolo. (**c**) Model of Piccolo C_2A domain with three bound Ca^{2+} ions on top (green spheres). The top surface of C_2A domain shows the binding sites for the headgroups of PIs. (**d**) Surface plot showing the electrostatic potential of C_2A domain. Blue, positive; red, negative charge; white, neutral. PIP_2 is pointed. (**e**) Space-filling model of PIP_2 is shown on top in pink C_2A domain, which provides a cupped shape of polybasic region to accommodate PIP_2.

positively charged residues in proteins and the negatively charged headgroups of PIs. The lowest binding energies of Piccolo C_2A domain for PI, PIP and PIP_2 with Ca^{2+} docking were −59.491, −93.229 and −102.642 Kcal, respectively, suggesting a specific interaction between PIP_2 and C_2A domain. Furthermore, the space-filling model showed that PIP_2 is tightly packed against the top surface of C_2A domain, which forms a favorable pocket to accommodate the moiety of PIP_2 (Figure 7e).

Piccolo regulated DAT function not through syntaxin 1A

As syntaxin 1A has been demonstrated to regulate the expressions and activities of serotonin transporter (SERT) and γ-aminobutyric acid (GABA) transporters,[23,24] Piccolo might regulate DAT surface expression through interaction with syntaxin 1A. We first investigated whether syntaxin 1A could bind to Piccolo, though syntaxin is identified to bind to Piccolo.[25] The lysates from hDAT-PC12 cells were immunoprecipitated with anti-syntaxin 1A, followed by hDAT immunoblotting. As shown in Supplementary Figure 1a, hDAT were present in the lysate. As expected, we also detected co-immunoprecipitation of hDAT and syntaxin 1A in following immunoprecipitation with anti-hDAT (Supplementary Figure 1b). These results showed an apparent association of these two molecules, which was supported by previous reports.[26] We then investigated whether syntaxin 1A could regulate DAT activity. The hDAT-PC12 cells were pretreated with Bont/C1, a toxin that specifically cleaves syntaxin 1A, followed by

[^{3}H]DA uptake assay; moreover, Bont/B that specifically cleaves the vesicle *N*-ethylmaleimide-sensitive factor attachment receptor protein synaptobrevin was used as a control. As shown in Supplementary Figure 1c, Bont/C1 (0.5–5 nM) failed to alter the [^{3}H]DA uptake in the cells treated with saline. Although Bont/C1 slightly elevated [^{3}H]DA uptake in the cells exposed to METH compared with Bont/B, the difference was not significant. To exclude that such incapability of Bont/C1 in modulating DA uptake was a result of the low concentration or short exposure time, we treated the cells with Bont/C1 at 0.25 μM for 6 h. However, [^{3}H]DA uptake was also not altered (data not shown). Additionally, exposure of METH at the concentration ranging from 0.5–20 μM for 30 min did not alter the expression level of syntaxin 1A in hDAT-PC12 cells (data not shown). Taken together, these data suggest that DAT and syntaxin 1A may mechanically, but not functionally, interact. Given the incapability of syntaxin 1A itself in modulating DAT, it unlikely mediates the role of Piccolo in regulating DAT expression at plasma membrane.

Discussion

The contribution of dopaminergic transmission to behavioral sensitization has been well recognized. Expression of certain proteins appears to be compensatory adaptation to the excessive DA signaling, which could be biologically adaptive mechanisms contributing to addiction. Nevertheless, some proteins likely function in a reverse manner. For example, we have previously found that the expression of tissue plasminogen activator plays a positive role in morphine-induced synaptic plasticity,[19] whereas tumor necrosis factor-α expression in NAc inhibits METH-induced dependence.[18] Piccolo expression was upregulated by repeated METH administration and partial knockdown of Piccolo expression by antisense technique led to elevated synaptic DA concentration in the NAc and two major behavioral manifestations in mice: heightened hyperlocomotor activity and rewarding effect. These findings strongly show that Piccolo overexpression elicited by METH may serve as a homeostatic mechanism that prevents behavioral sensitization by maintaining the expression and activity of the plasmalemmal DAT.

The human Piccolo gene contains more than 25 exons spanning over 350 kb of genomic DNA maps to 7q11.23-q21.3, a region of chromosome 7 implicated as a linkage site for autism and Williams Syndrome.[22] Therefore, dysfunction of Piccolo may be involved in cognitive impairment and mental retardation.[27] The mechanism underlying Piccolo upregulation caused by METH remains to be elucidated. Nevertheless, inhibitory feedback to the excessive DA signaling would be a plausible candidate.

Piccolo has been reported to localize at the GABAergic and glycinergic presynaptic terminal,[10] and our findings in immunostaining demonstrated that it is also expressed at dopaminergic presynaptic terminal. DAT can be internalized from the plasma membrane at a relatively rapid rate, which provides a mechanism by which the turnover rate and density of the plasmalemmal DAT can be quickly and finely modulated.[6,8] Signaling molecules, glycosylation and DAT substrates have been shown to regulate DAT membrane trafficking. Given those findings *in vivo* behaviors tests and the properties of Piccolo, we assumed that Piccolo may play a role in modulating DA flux and DAT distribution at dopaminergic terminals. To address this issue, we investigated DA uptake and membrane DAT expression in hDAT-PC12 cells expressing different functional domain of Piccolo. METH caused DA uptake inhibition in parallel with decreased DAT surface expression, which was well consistent with those works defining the dynamically internalized DAT in hDAT-PC12 cells triggered by amphetamine. These results further support the notion that redistribution of surface DAT caused by METH-like drugs may present an important mechanism underlying the consequently reduced DAT activity. Our data showed that Piccolo C_2A, but not PDZ domain, attenuated METH-induced DA uptake inhibition by retaining DAT expression at cell surface. Because DAT can be internalized and/or recycled, we speculated that the decreased loss of membrane DAT could be resulted from attenuated DAT internalization. Such hypothesis was demonstrated by reversible biotinylation, which revealed the decreased DAT internalization in C_2A domain-transfected cells responding to METH.

It is well established that PIP_2 functions in regulating cytoskeleton, channels and transporters, and membrane trafficking at presynaptic terminal.[16,28,29] Especially, PIP_2 is essential at several stages of endocytosis for the sequential recruitment of adaptor and accessory proteins to endocytic sites.[30,31] METH rapidly causes both DAT internalization and conformational rearrangement to an intracellularly oriented transporter from which DA is released. Such process is proposed to be a drastic membrane movement and requires PIP_2 to assemble various molecules to form endocytic compartment. Significantly, we found that PIP_2 exhibits a similar distribution pattern with DAT at membrane microdomains. Furthermore, internalized DTA triggered by METH is accompanied with PIP_2 in endocytic compartments. These results indicate that PIP_2 is an important regulator in the process of DAT internalization.

A couple of scaffolding proteins such as GAP43, CAP23 and Dap160 have shown their ability to sequester membrane PIP_2, thus potentially modulating the endocytic process.[32,33] In this study we obtained several evidences further supporting the notion that Piccolo can electrostatically sequester PIP_2. Firstly, Piccolo C_2A domain may laterally bind membrane PIP_2, and augment PIP_2 clusters in hDAT-PC12 cells. In principle, the augmented clusters could represent the sequestration of phospholipids like PIP_2 at the plasma membrane.[34] Secondly, the crystal

packing contacts for PIP_2 were the clusters of basic/aromatic residues, which exhibit a universal capability of sequestering membrane PIP_2.[35] Thirdly, the space-filling model showed that Piccolo C_2A domain may pocket PIP_2 by a cupped shape of polybasic region, where the local positive potential electrostatically attracts the negatively charged PIP_2. Finally, C_2A domain shows stronger interacting potential with PIP_2 than PI or PIP. Our results are consistent with previous investigations indicating that PIs binding with Piccolo C_2A domain is largely driven by electrostatic interaction.[15]

Based on these findings, we speculated that Piccolo C_2A domain may regulate METH-triggered DAT internalization through sequestering PIP_2, and the findings in immunostaining strongly support this prediction. Piccolo C_2A domain mainly anchors nonuniformly to the inner leaflet, which is accompanied with the retention of DAT and PIP_2 at membrane microdomains; moreover, it clearly attenuated METH-triggered DAT and PIP_2 internalization in cytosol. These results show that Piccolo may sequester or 'control' locally PIP_2 by C_2A domain in membrane raft and suppress PIP_2-dependent endocytic process, thus leading to the attenuated DAT internalization.

How does the Piccolo C_2A domain–PIP_2 interaction fulfill a function in modulating DAT internalization and psychostimulant responsiveness? An explanation could be that the endocytic process for DAT internalization is inhibited directly through PIP_2 sequestration. Given the strong dependence of the endocytic machinery on PIP_2, more membrane PIP_2 is considerably mobilized for the accelerated DAT internalization triggered by METH. This situation would place the endocytic machinery of dopaminergic presynaptic terminal in a compromised position of insufficient availability of PIP_2, and thus slowing down the DAT internalization. Similarly, a dominant-negative mutant of dynamin I, a component of endocytic machinery, inhibits both PKC- and amphetamine-dependent DAT internalization;[7,36] interruption of adaptor proteins present in clathrin-coated pits like epsin interferes with DAT endocytosis.[37] Another explanation could be that Piccolo C_2A domain may retain DAT at cell surface by promoting membrane stability. METH causes both DAT internalization and conformational rearrangement to an intracellularly oriented transporter from which DA is released. In this process PIP_2 acts as a positive regulator in modulating actin filament assembly and membrane movement by creating membrane microdomains and binding proteins with lipid-specific interaction.[38,39] Therefore, overexpressed Piccolo elicited by METH may enhance the association with membrane PIP_2 or other PIs through C_2A domain and disturb PIP_2-dependent actin assembly, thereby strengthening membrane stability and weakening DAT internalization. In this case, Piccolo may function as a general stabilizer for plasma membrane and DAT. It is worth noting that protein interacting with C kinase 1 (PICK1), a skeletal component, may also stabilize and maintain DAT at plasma membrane.[40]

Piccolo likely binds to syntaxin 1A through its C_2A domain, because synaptotagmin C_2A domain which shares a great structural similarity with Piccolo C_2A domain interacts with syntaxin 1A.[15,40] Syntaxin 1A directly regulates the expressions and activities of SERT and GABA transporter.[23,24] Interestingly, a recent work has identified that syntaxin 1A also binds to DAT.[26] However, Piccolo C_2A domain appears not to regulate METH-induced DAT internalization through syntaxin 1A, because DA uptake is not affected when syntaxin 1A is inhibited.

Our findings reveal that Piccolo is capable of regulating METH-induced DAT internalization, leading to the change of DA signaling and synaptic strength. The precise mechanism underlying the role of C_2A domain–PIP_2 interplay in DAT internalization remains to be determined. No matter which mechanism could be more reasonable, sequestration of PIP_2 in lateral domains through C_2A domain appears to be important for Piccolo to regulate DAT internalization. Therefore, a greater understanding of the molecular regulators for PIP_2, which governs DAT trafficking, would shed light on the modulation of DAT surface presentation. Further investigation measuring membrane fluorescence resonance energy transfer and PIP_2 turnover/mobilization will help interpret the contribution of the proposed mechanisms.

The present investigation illustrates a paradigm that Piccolo, a presynaptic scaffolding protein, targets membrane PIP_2 by its C_2A domain, contributing to the regulation of DAT internalization. Piccolo upregulation may represent a homeostatic response of dopaminergic neurons in the NAc to excessive dopaminergic transmission, dampening hypersensitivity and rewarding effect.

Acknowledgments

We are thankful to Dr Seino Susumu and Dr Shibasaki Takao (Division of Cellular and Molecular Medicine, Kobe University Graduate School of Medicine, Japan) for the kind gifts of pCMV-HA-Piccolo-PDZ, pCMV-Myc-Piccolo-C_2A and pGEX4T-GST-p13192. We thank Mrs Nobushi Hamada and Yoshiyuki Nakamura radioisotope Center Medical Branch, Nagoya University School of Medicine for technical support. This study was supported in part by a Grant-in-Aid for Science Research and Special Coordination Funds for Promoting Science and Technology, Target-Oriented Brain Science Research Program and 21st Century Center of Excellence Program 'Integrated Molecular Medicine for Neuronal and Neoplastic Disorders' and 'Academic Frontier Project for Private Universities (2007–2011), from the Ministry of Education, Culture, Sports, Science and Technology of Japan; by a Grant-in-Aid for Health Science Research on Regulatory Science of Pharmaceuticals and Medical Devices, and Comprehensive Research on Aging and Health from the

Ministry of Health, Labor and Welfare of Japan; by a Smoking Research Foundation Grant for Biomedical Research and Takeda Science Foundation.

References

1 Kahlig KM, Binda F, Khoshbouei H, Blakely RD, McMahon DG, Javitch JA *et al.* Amphetamine induces dopamine efflux through a dopamine transporter channel. *Proc Natl Acad Sci USA* 2005; **102**: 3495–3500.
2 Sulzer D, Chen TK, Lau YY, Kristensen H, Rayport S, Ewing A. Amphetamine redistributes dopamine from synaptic vesicles to the cytosol and promotes reverse transport. *J Neurosci* 1995; **15**: 4102–4108.
3 Sandoval V, Riddle EL, Ugarte YV, Hanson GR, Fleckenstein AE. Methamphetamine-induced rapid and reversible changes in dopamine transporter function: an *in vitro* model. *J Neurosci* 2001; **21**: 1413–1419.
4 Holton KL, Loder MK, Melikian HE. Nonclassical, distinct endocytic signals dictate constitutive and PKC-regulated neurotransmitter transporter internalization. *Nat Neurosci* 2005; **8**: 881–888.
5 Sorkina T, Hoover BR, Zahniser NR, Sorkin A. Constitutive and protein kinase C-induced internalization of the dopamine transporter is mediated by a clathrin-dependent mechanism. *Traffic* 2005; **6**: 157–170.
6 Loder MK, Melikian HE. The dopamine transporter constitutively internalizes and recycles in a protein kinase C-regulated manner in stably transfected PC12 cell lines. *J Biol Chem* 2003; **278**: 22168–22174.
7 Saunders C, Ferrer JV, Shi L, Chen J, Merrill G, Lamb ME *et al.* Amphetamine-induced loss of human dopamine transporter activity: an internalization-dependent and cocaine-sensitive mechanism. *Proc Natl Acad Sci USA* 2000; **97**: 6850–6855.
8 Sorkina T, Doolen S, Galperin E, Zahniser NR, Sorkin A. Oligomerization of dopamine transporters visualized in living cells by fluorescence resonance energy transfer microscopy. *J Biol Chem* 2003; **278**: 28274–28283.
9 Zhai RG, Vardinon-Friedman H, Cases-Langhoff C, Becker B, Gundelfinger ED, Ziv NE *et al.* Assembling the presynaptic active zone: a characterization of an active one precursor vesicle. *Neuron* 2001; **29**: 131–143.
10 Fenster SD, Chung WJ, Zhai R, Cases-Langhoff C, Voss B, Garner AM *et al.* Piccolo, a presynaptic zinc finger protein structurally related to bassoon. *Neuron* 2000; **25**: 203–214.
11 Fenster SD, Kessels MM, Qualmann B, Chung WJ, Nash J, Gundelfinger ED *et al.* Interactions between Piccolo and the actin/dynamin-binding protein Abp1 link vesicle endocytosis to presynaptic active zones. *J Biol Chem* 2003; **278**: 20268–20277.
12 Wang X, Kibschull M, Laue MM, Lichte B, Petrasch-Parwez E, Kilimann MW. Aczonin, a 550-kD putative scaffolding protein of presynaptic active zones, shares homology regions with Rim and Bassoon and binds profilin. *J Cell Biol* 1999; **147**: 151–162.
13 Garner CC, Nash J, Huganir RL. PDZ domains in synapse assembly and signaling. *Trends Cell Biol* 2000; **10**: 274–280.
14 Garcia J, Gerber SH, Sugita S, Sudhof TC, Rizo J. A conformational switch in the Piccolo C2A domain regulated by alternative splicing. *Nat Struct Mol Biol* 2004; **11**: 45–53.
15 Gerber SH, Garcia J, Rizo J, Sudhof TC. An unusual C(2)-domain in the active-zone protein piccolo: implications for Ca(2+) regulation of neurotransmitter release. *EMBO J* 2001; **20**: 1605–1619.
16 Cremona O, De Camilli P. Phosphoinositides in membrane traffic at the synapse. *J Cell Sci* 2001; **114**: 1041–1052.
17 Fujimoto K, Shibasaki T, Yokoi N, Kashima Y, Matsumoto M, Sasaki T *et al.* Piccolo, a Ca^{2+} sensor in pancreatic beta-cells. Involvement of cAMP-GEFII.Rim2.Piccolo complex in cAMP-dependent exocytosis. *J Biol Chem* 2002; **277**: 50497–50502.
18 Nakajima A, Yamada K, Nagai T, Uchiyama T, Miyamoto Y, Mamiya T *et al.* Role of tumor necrosis factor-alpha in methamphetamine-induced drug dependence and neurotoxicity. *J Neurosci* 2004; **24**: 2212–2225.
19 Nagai T, Yamada K, Yoshimura M, Ishikawa K, Miyamoto Y, Hashimoto K *et al.* The tissue plasminogen activator-plasmin system participates in the rewarding effect of morphine by regulating dopamine release. *Proc Natl Acad Sci USA* 2004; **101**: 3650–3655.
20 Melikian HE, Buckley KM. Membrane trafficking regulates the activity of the human dopamine transporter. *J Neurosci* 1999; **19**: 7699–7710.
21 Bowers MS, McFarland K, Lake RW, Peterson YK, Lapish CC, Gregory ML *et al.* Activator of G protein signaling 3: a gatekeeper of cocaine sensitization and drug seeking. *Neuron* 2004; **42**: 269–281.
22 Fenster SD, Garner CC. Gene structure and genetic localization of the PCLO gene encoding the presynaptic active zone protein Piccolo. *Int J Dev Neurosci* 2002; **20**: 161–171.
23 Quick MW. Regulating the conducting states of a mammalian serotonin transporter. *Neuron* 2003; **40**: 537–549.
24 Deken SL, Beckman ML, Boos L, Quick MW. Transport rates of GABA transporters: regulation by the N-terminal domain and syntaxin 1A. *Nat Neurosci* 2002; **3**: 998–1003.
25 Shapira M, Zhai RG, Dresbach T, Bresler T, Torres VI, Gundelfinger ED *et al.* Unitary assembly of presynaptic active zones from Piccolo-Bassoon transport vesicles. *Neuron* 2003; **38**: 237–252.
26 Lee KH, Kim MY, Kim DH, Lee YS. Syntaxin 1A and receptor for activated C kinase interact with the N-terminal region of human dopamine transporter. *Neurochem Res* 2004; **29**: 1405–1409.
27 Weidenhofer J, Bowden NA, Scott RJ, Tooney PA. Altered gene expression in the amygdala in schizophrenia: up-regulation of genes located in the cytomatrix active zone. *Mol Cell Neurosci* 2006; **31**: 243–250.
28 Suh BC, Hille B. Regulation of ion channels by phosphatidylinositol 4,5-bisphosphate. *Curr Opin Neurobiol* 2005; **15**: 370–378.
29 Kanzaki M, Furukawa M, Raab W, Pessin JE. Phosphatidylinositol 4,5-bisphosphate regulates adipocyte actin dynamics and GLUT4 vesicle recycling. *J Biol Chem* 2004; **279**: 30622–30633.
30 Slepnev VI, De Camilli P. Accessory factors in clathrin-dependent synaptic vesicle endocytosis. *Nat Rev Neurosci* 2000; **1**: 161–172.
31 Itoh T, Koshiba S, Kigawa T, Kikuchi A, Yokoyama S, Takenawa T. Role of the ENTH domain in phosphatidylinositol-4,5-bisphosphate binding and endocytosis. *Science* 2001; **291**: 1047–1051.
32 Laux T, Fukami K, Thelen M, Golub T, Frey D, Caroni P. GAP43, MARCKS, and CAP23 modulate PI(4,5)P(2) at plasmalemmal rafts, and regulate cell cortex actin dynamics through a common mechanism. *J Cell Biol* 2000; **86**: 2188–2207.
33 Marie B, Sweeney ST, Poskanzer KE, Roos J, Kelly RB, Davis GW. Dap160/intersectin scaffolds the periactive zone to achieve high-fidelity endocytosis and normal synaptic growth. *Neuron* 2004; **43**: 207–219.
34 Kwik J, Boyle S, Fooksman D, Margolis L, Sheetz MP, Edidin M. Membrane cholesterol, lateral mobility, and the phosphatidylinositol 4,5-bisphosphate-dependent organization of cell actin. *Proc Natl Acad Sci USA* 2003; **100**: 13964–13969.
35 Daniels GM, Amara SG. Regulated trafficking of the human dopamine transporter-clathrin-mediated internalization and lysosomal degradation in response to phorbol esters. *J Biol Chem* 1999; **274**: 35794–35801.
36 Sorkina T, Miranda M, Dionne KR, Hoover BR, Zahniser NR, Sorkin A. RNA interference screen reveals an essential role of Nedd4-2 in dopamine transporter ubiquitination and endocytosis. *J Neurosci* 2006; **26**: 8195–8205.
37 Nebl T, Oh SW, Luna EJ. Membrane cytoskeleton: PIP(2) pulls the strings. *Curr Biol* 2000; **10**: R351–R354.
38 Gruenberg J. Lipids in endocytic membrane transport and sorting. *Curr Opin Cell Biol* 2003; **15**: 382–388.
39 Torres GE, Yao WD, Mohn AR, Quan H, Kim KM, Levey AI *et al.* Functional interaction between monoamine plasma membrane transporters and the synaptic PDZ domain-containing protein PICK1. *Neuron* 2001; **30**: 121–134.
40 Shao X, Li C, Fernandez I, Zhang X, Sudhof TC, Rizo J. Synaptotagmin-syntaxin interaction: the C2 domain as a Ca2+-dependent electrostatic switch. *Neuron* 1997; **18**: 133–142.

Supplementary Information accompanies the paper on the Molecular Psychiatry website (http://www.nature.com/mp)

Molecular Psychiatry (2008) 13, 349

www.nature.com/mp

IMAGE

Piccolo regulates dopamine transporter internalization via PIP_2

X Cen[1,2], A Nitta[1], D Ibi[1,3], Y Zhao[1], M Niwa[1], K Taguchi[1], M Hamada[1], Y Ito[3], Y Ito[4], L Wang[2] and T Nabeshima[1,5]

[1]*Department of Neuropsychopharmacology and Hospital Pharmacy, Nagoya University Graduate School of Medicine, Nagoya, Japan;* [2]*National Chengdu Center for Safety Evaluation of Drugs, West China Hospital, Sichuan University, Chengdu, China;* [3]*Department of Pharmacology, College of Pharmacy, Nihon University, Chiba, Japan;* [4]*Equipment Center for Research and Education, Nagoya University Graduate School of Medicine, Nagoya, Japan and* [5]*Department of Chemical Pharmacology, Meijo University Graduate School of Pharmaceutical Sciences, Nagoya, Japan*

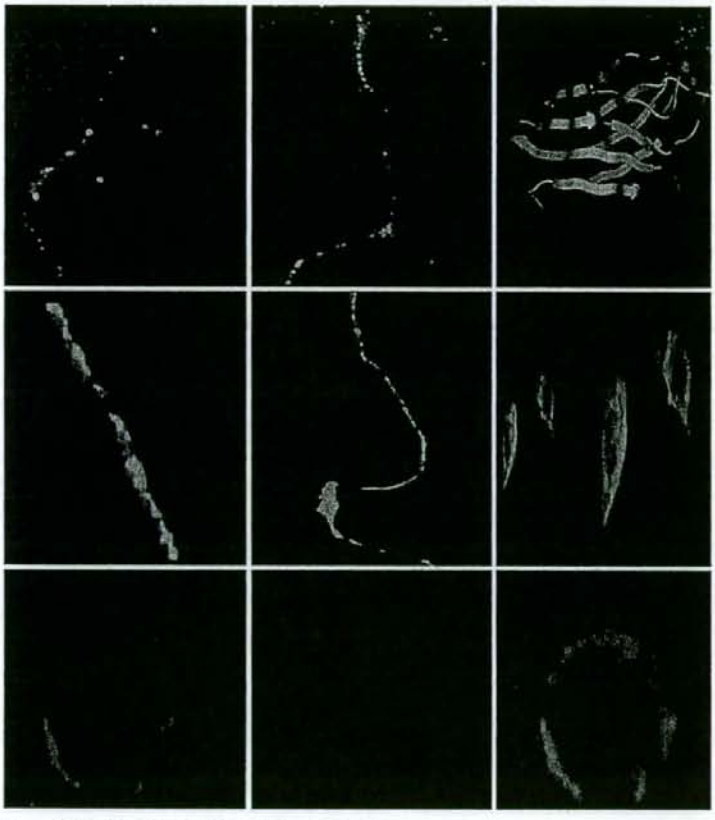

Molecular Psychiatry (2008) **13,** 349; doi:10.1038/mp.2008.17

Two left upper panels show that piccolo is not colocalized with tyrosine hydroxyls (TH)-positive neurons. Two left middle panels show that piccolo is colocalized with dopamine transporter (DAT)-positive neurons. Bottom three panels show piccolo C2A domain (left; green), dopamine transporter (middle; red) and merge image (right). Most upper right panel is docking simulation between piccolo C2A domain and PIP_2 under Ca^{2+} present condition. The right middle panel shows the piccolo C2A domain is colocalized with dopamine transporter in normal condition. For more information on this topic see the paper by Cen *et al.* on pages 451–463.

Neuropsychopharmacology (2008), 1–15

www.neuropsychopharmacology.org

Antiamnesic and Neuroprotective Effects of the Aminotetrahydrofuran Derivative ANAVEX1-41 Against Amyloid β_{25-35}-Induced Toxicity in Mice

Vanessa Villard[1,2,3], Julie Espallergues[1,2,3], Emeline Keller[1,2,3], Tursun Alkam[4,5], Atsumi Nitta[4], Kiyofumi Yamada[4], Toshitaka Nabeshima[4,6], Alexandre Vamvakides[7] and Tangui Maurice*[,1,2,3]

[1]INSERM U.710, Montpellier, France; [2]University of Montpellier 2, Montpellier, France; [3]EPHE, Paris, France; [4]Department of Neuropsychopharmacology and Hospital Pharmacy, Nagoya University Graduate School of Medicine, Nagoya, Japan; [5]Department of Basic Medicine, College of Traditional Uighur Medicine, Hotan, China; [6]Department of Chemical Pharmacology, Graduate School of Pharmaceutical Science, Meijo University, Nagoya, Japan; [7]Anavex Life Sciences, Pallini, Greece

The antiamnesic and neuroprotective activities of the new aminotetrahydrofuran derivative tetrahydro-*N,N*-dimethyl-5,5-diphenyl-3-furanmethanamine hydrochloride (ANAVEX1-41), a nonselective muscarinic receptor ligand and σ_1 protein activator, were examined in mice injected intracerebroventricularly with amyloid β_{25-35} ($A\beta_{25-35}$) peptide (9 nmol). $A\beta_{25-35}$ impaired significantly spontaneous alternation performance, a spatial working memory, and passive avoidance response. When ANAVEX1-41 (1–1000 μg/kg i.p.) was administered 7 days after $A\beta_{25-35}$, ie, 20 min before the behavioral tests, it significantly reversed the $A\beta_{25-35}$-induced deficits, the most active doses being in the 3–100 μg/kg range. When the compound was preadministered 20 min before $A\beta_{25-35}$, ie, 7 days before the tests, it prevented the learning impairments at 30–100 μg/kg. Morphological analysis of corticolimbic structures showed that $A\beta_{25-35}$ induced a significant cell loss in the CA1 pyramidal cell layer of the hippocampus that was prevented by ANAVEX1-41 (100 μg/kg). Increased number of glial fibrillary acidic protein immunopositive cells in the retrosplenial cortex or throughout the hippocampus revealed an $A\beta_{25-35}$-induced inflammation that was prevented by ANAVEX1-41. The drug also prevented the parameters of $A\beta_{25-35}$-induced oxidative stress measured in hippocampus extracts, ie, the increases in lipid peroxidation and protein nitration. ANAVEX1-41, however, failed to prevent $A\beta_{25-35}$-induced caspase-9 expression. The compound also blocked the $A\beta_{25-35}$-induced caspase-3 expression, a marker of apoptosis. Both the muscarinic antagonist scopolamine and the σ_1 protein inactivator BD1047 prevented the beneficial effects of ANAVEX1-41 (30 or 100 μg/kg) against $A\beta_{25-35}$-induced learning impairments, suggesting that muscarinic and σ_1 targets are involved in the drug effect. A synergic effect could indeed account for the very low active doses measured *in vivo*. These data outline the therapeutic potential of ANAVEX1-41 as a neuroprotective agent in Alzheimer's disease.
Neuropsychopharmacology advance online publication, 3 December 2008; doi:10.1038/npp.2008.212

Keywords: amyloid toxicity; σ_1 protein ligand; muscarinic ligand; oxidative stress; learning and memory

INTRODUCTION

Alzheimer disease (AD) is an irreversible, progressive and degenerative disorder damaging the higher structures of the brain (Selkoe, 1989, 2004). It is actually incurable, as the available treatments, acetylcholinesterase inhibitors or a *N*-methyl-D-aspartate receptor antagonist with neuroprotective potential, memantine, are mainly symptomatic. The pathological cleavage of amyloid precursor protein (APP) is responsible for the accumulation of amyloid-β ($A\beta$) proteins, aggregating into fibrillar oligomers and generating amyloid deposits that, in turn, form the senile plaques (Selkoe, 1989, 2004). Oligomers of $A\beta$ peptides are considered as the main factor mediating the devastating neurotoxicity observed in AD. $A\beta$ peptides vary in length from 40 to 43 amino acids, $A\beta_{1-42}$ occurring more frequently and forms fibrillar aggregates far more readily than $A\beta_{1-40}$ or $A\beta_{1-43}$ (Selkoe, 1989). Minor fragments were also identified including the highly toxic $A\beta_{25-35}$ peptide (Kubo *et al*, 2002; Gruden *et al*, 2007). The $A\beta$-mediated toxicity follows a very complex pattern. $A\beta$ oligomers form Ca^{2+} permeable pores on plasma membranes and interact with intracellular organelles regulating calcium homeostasis, the endoplasmic reticulum (ER) and mitochondria (Abramov *et al*, 2004), provoking a massive oxidative stress

*Correspondence: Dr T Maurice, INSERM U.710, EPHE, University of Montpellier II, c.c. 105, place Eugène Bataillon, 34095 Montpellier cedex 5, France, Tel: +33 4 67 14 36 23, Fax: +33 4 67 14 33 86, E-mail: Tangui.Maurice@univ-montp2.fr
Received 25 July 2008; revised 21 October 2008; accepted 22 October 2008

and induction of neuronal apoptotic death. $A\beta$ proteins are also responsible for a generalized inflammatory response in brain structures associated with production of cytokines by activated astroglia and microglia (Frederickson, 1992) and exacerbated excitotoxic processes (Mattson *et al*, 1992).

Moreover, toxicity of $A\beta$ has recently been shown to be highly dependent on the aggregation species (Chafekar *et al*, 2008). $A\beta$ can exist in different assembly states and apart from the monomeric and mature fibrillar stages, different intermediate species have been identified, such as low molecular weight oligomers, larger globular oligomers, and protofibrils. This is true for $A\beta_{1-40}$ or $A\beta_{1-42/3}$ but also for $A\beta_{25-35}$ peptide. These different species greatly differ in their neurotoxic potential and molecular mechanism mediating the toxicity. For instance, impairment of long-term potentiation (Walsh *et al*, 2002) and ER stress (Chafekar *et al*, 2007) may be mediated by small oligomers, whereas the neuroinflammatory response may rather involve fibrillar $A\beta$ (Eikelenboom *et al*, 2002). Preliminary observations of the laboratory showed that after *in vitro* aggregation, $A\beta_{25-35}$ peptide exist in these different species including small oligomers, amorphous oligomers, and fibrillar forms (S Marchal, L Givalois, T Maurice, unpublished work).

We described the nontransgenic model of AD induced in rodents by injection into the lateral ventricle of aggregated $A\beta_{25-35}$ peptide (Maurice *et al*, 1996; Delobette *et al*, 1997). The morphological and biochemical characterization of amyloid toxicity induced by $A\beta_{25-35}$ has been subsequently analyzed in details. $A\beta_{25-35}$ induces brain inflammation, oxidative stress, activation of proapoptotic caspases, impairment of long-term potentiation, cell loss in the hippocampus, and memory impairments (Stepanichev *et al*, 2004, 2006; Meunier *et al*, 2006). Recently, it was also observed that $A\beta_{25-35}$ injection activates the glycogen synthase kinase-3β, involved in cell survival regulation, T-phosphorylation and APP processing, suggesting that acute $A\beta_{25-35}$ injection results in production and seeding of endogenous $A\beta_{1-40/42}$ and T-phosphorylation (Klementiev *et al*, 2007). The model therefore appears as highly suitable to analyze the putative antiamnesic and neuroprotective activity of drugs with potential interest in AD, as recently used by several authors (Fang and Liu, 2006; Kuboyama *et al*, 2006; Meunier *et al*, 2006; Um *et al*, 2006; Alkam *et al*, 2007).

The σ_1 protein has only recently been identified as a chaperone protein located on membranes forming focal contacts between the ER and mitochondria (Hayashi and Su, 2007). In basal conditions, the σ_1 protein forms a complex with the other chaperone glucose-regulated protein 78 kDa (GRP78/BiP). Upon ER Ca^{2+} depletion or by ligand stimulation, the σ_1 protein dissociates from GRP78/BiP, leading to a prolonged Ca^{2+} signaling into mitochondria by IP_3 receptors (Hayashi and Su, 2007). Under intracellular Ca^{2+} signaling disruption and subsequent ER stress, the σ_1 protein translocates, to reach plasma membrane, recruiting Ca^{2+}-dependent intracellular cascades (Morin-Surun *et al*, 1999). On the plasma membrane, it contributes to form or modify the composition of lipid-rich microdomains, so-called lipid rafts (Hayashi and Su, 2001, 2003). Increasing or activating σ_1 proteins is expected to counteract ER stress response, whereas decreasing or inactivating them would enhance apoptosis (Hayashi and Su, 2007). Modifying σ_1 protein activation using selective activators/agonists therefore mediates a unique pharmacological action on Ca^{2+} homeostasis and signal transduction pathways, which has proven to allow an effective neuroprotection against several kinds of insults, including excitotoxicity, oxidative stress, and amyloid toxicity (for reviews, see Maurice *et al*, 2006; Monnet and Maurice, 2006). Indeed, preliminary experiments showed that, *in vitro*, the selective σ_1 activators PRE-084 and MR-22 attenuate the $A\beta_{25-35}$-induced expression of the proapoptotic protein Bax and neuronal death in rat cortical cultures (Marrazzo *et al*, 2005). We reported that, *in vivo*, PRE-084 prevents the $A\beta_{25-35}$-induced oxidative stress and learning impairments in mice (Meunier *et al*, 2006).

ANAVEX1-41 is a new aminotetrahydrofuran derivative (Vamvakides, 2002; Espallergues *et al*, 2007) acting as a σ_1 protein activator, with a high affinity (44 nM) and selectivity. The CEREP profile of the compound showed that it also presents nanomolar affinities (18–114 nM) for muscarinic receptors ($M_1 > M_3$, $M_4 > M_2$), some low micromolar affinity for sodium channel site 2, and negligible interaction with 60 other receptor and enzyme assays (data not shown). Its molecular profile is coherent with its antiamnesic and antidepressant effects (Espallergues *et al*, 2007). In this study, we analyzed its antiamnesic and neuroprotective potentials against $A\beta_{25-35}$-induced toxicity in mice. Learning deficits were measured using the spontaneous alternation test measuring spatial working memory and passive avoidance response measuring long-term contextual memory. The $A\beta_{25-35}$-induced toxicity was also analyzed at the morphological and biochemical levels. Finally, the involvement of the σ_1 protein or muscarinic receptors was examined using pretreatments with a selective antagonist, BD1047 or scopolamine, respectively.

MATERIALS AND METHODS

Animals

Male Swiss mice (Depré, St-Doulchard, France), aged 7 weeks and weighing 32 ± 2 g, were used in this study. Animals were housed in plastic cages in groups. They had free access to food and water, except during behavioral experiments, and they were kept in a regulated environment (23 ± 1°C, 40–60% humidity) under a 12 h light/dark cycle (light on at 0800 hours). Experiments were carried out between 0900 and 1700 hours, in an experimental room within the animal facility. Mice were habituated 30 min before each experiment. All animal procedures were conducted in strict adherence of European Union Directive of 24 November 1986 (86–609).

Drugs

Tetrahydro-*N*,*N*-dimethyl-5,5-diphenyl-3-furanmethanamine hydrochloride (ANAVEX1-41, formerly AE14) was synthesized in the laboratory (Anavex Life Sciences, Pallini, Greece). *N*-[2-(3,4-dichlorophenyl)ethyl]-*N*-methyl-2-(dimethylamino)ethylamine dihydrobromide (BD1047) was from Tocris Bioscience (Bristol, UK). All other materials, including scopolamine hydrobromide, xylenol orange, and cumene peroxide, were purchased from Sigma-Aldrich (Saint Quentin Fallavier, France). Drugs used for *in vivo*

experiments were solubilized in physiological saline solution and administered intraperitoneally (i.p.) in a volume of 100 µl per 20 g body weight. The $A\beta_{25-35}$ peptide (Gly-Ser-Asn-Lys-Gly-Ala-Ile-Ile-Gly-Leu-Met, $A\beta_{25-35}$) and scrambled $A\beta_{25-35}$ peptide (Ala-Lys-Ile-Gly-Asn-Ser-Ile-Gly-Leu-Met-Gly, Sc$A\beta$) were from NeoMPS (Strasbourg, France). They were dissolved in sterile bidistilled water at a concentration of 3 mg/ml and stored at −20°C until use. Before injection, peptides were aggregated by incubation at 3 mg/ml in sterile bidistilled water at 37°C for 4 days. They were administered intracerebroventricularly (i.c.v.) in a final volume of 3 µl per mouse, as previously described (Maurice *et al*, 1996, 1998).

Spontaneous Alternation Performances

Each mouse, naive to the apparatus, was placed at the end of one arm in a *Y*-maze (three arms, 40 cm long, 120° separate) and allowed to move freely through the maze during a single 8-min session. The series of arm entries, including possible returns into the same arm, was recorded visually. An alternation was defined as entries into all three arms on consecutive trials. The number of the total possible alternations was therefore the total number of arm entries minus two and the percentage of alternation was calculated as (actual alternations/total possible alternations) × 100. Animals performing less than eight arm entries in 8 min were discarded (ie, less than 5% of animals).

Step-Down Type Passive Avoidance Test

The apparatus consisted of a transparent acrylic cage (30 × 30 × 40 cm high) with a grid-floor, inserted in a soundproof outer box (35 × 35 × 90 cm high). A 15 W lamp lighted the cage during the experimental period. A wooden platform (4 × 4 × 4 cm) was fixed at the center of the grid-floor. Intermittent electric shocks (1 Hz, 500 ms, 40 V DC) were delivered to the grid-floor using an isolated pulse stimulator (Model 2100; AM Systems, Everett, WA, USA). The test consisted of two training sessions, at 90-min time interval, and a retention session, carried out 24 h after the first training. During training sessions, each mouse was placed on the platform. When it stepped down and placed its four paws on the grid-floor, shocks were delivered for 15 s. Step-down latency and the numbers of vocalizations and flinching reactions were measured. Shock sensitivity was evaluated by adding these two numbers. None of the treatments used in this study significantly affected the shock sensitivity. Animals that stepped down before 3 s has elapsed or that did not step down within 30 s were discarded (ie, less than 5% of the mice). Animals, which did not step down within 60 s during the second session, were considered as remembering the task and taken off, without receiving further electric shocks. The retention test was performed in a similar manner as training, except that the shocks were not applied to the grid-floor. Each mouse was again placed on the platform, and the latency was recorded, with an upper cutoff time of 300 s. Two parametric measures of retention were analyzed: the latency and the number of animals reaching the avoidance criterion, defined as correct if the latency measured during the retention session was greater than threefold the latency showed by the animal during the second training session and, at least, greater than 60 s.

Histology

Each mouse was anesthetized by intramuscular (i.m.) injection of ketamine, 80 mg/kg, and xylazine, 10 mg/kg, and quickly transcardially perfused with 50 ml of saline solution followed by 50 ml of paraformaldehyde 4%. Brains were removed and kept overnight in the fixative solution. They were cut in coronal sections (30 µm thickness) using a vibratome (Leica VT1000 S). Serial sections were selected to include the hippocampus formation and placed in gelatin-coated glass strip. Sections were stained with 0.2% cresyl violet reagent (Sigma-Aldrich), then dehydrated with graded ethanol, treated with toluene and mounted with DePeX medium (BDH Laboratories, Poole, UK). Examination of the CA1 area was performed using a light microscope (Dialux 22, Leitz), slices being digitalized through a CCD camera (Sony XC-77CE) with the NIH ImageJ software, to easily process CA1 measurement and pyramidal cells counts. Data were calculated as average of six slices and expressed as number of viable CA1 pyramidal cells per millimeter for each group.

Immunohistochemistry

Mice were anesthetized by i.m. injection of ketamine 10% and xylazine 2%, perfused transcardially with 50 ml of saline solution followed by 50 ml of paraformaldehyde 4%. Brains were removed and kept overnight in the fixative solution. Brain sections were cut in coronal sections (30 µm thickness) using a vibratome (Leica VT1000 S). Analysis of the glial response to neurodegeneration was carried out by immunolabeling sections, with mouse monoclonal antiglial fibrillary acidic protein (GFAP; Sigma-Aldrich; 1 : 1000).

Lipid Peroxidation Measures

Mice were killed by decapitation and brains were rapidly removed, weighed, and kept in liquid nitrogen until assayed. After thawing, brains were homogenized in cold methanol (1 : 10, w/v), centrifuged at 1000 *g* during 5 min and the supernatant collected. Homogenate was added to a solution containing $FeSO_4$ 1 mM, H_2SO_4 0.25 M, xylenol orange 1 mM, and incubated for 30 min at room temperature. Absorbance was measured at 580 nm ($A_{580}1$), and 10 µl of cumene hydroperoxide (CHP) 1 mM was added to the sample and incubated for 30 min at room temperature, to determine the maximal oxidation level. Absorbance was measured at 580 nm ($A_{580}2$). The level of lipid peroxidation was determined as CHP equivalents according to: CHP equiv. = $A_{580}1/A_{580}2 \times$ (CHP (nmol)) × dilution, and expressed as CHP equiv. per wet tissue weight.

Western Blotting

For determination of protein nitration levels, mice were decapitated 5 days after $A\beta$ peptide injection. The hippocampus were removed on ice-cold glass plate and stored at −80°C. The hippocampus tissues were homo-

genized in ice-cold 20 mM Tris–HCl extraction buffer, pH 7.6, containing 150 mM NaCl, 2 mM EDTA, 50 mM sodium fluoride, 1 mM sodium vanadate, 1% NP-40, 1% sodium deoxycholate, 0.1% sodium dodecylsulfate (SDS), 1 mg/ml pepstatin, 1 mg/ml aprotinin, and 1 mg/ml leupeptin. Equal amounts of protein, 40 µg per lane, were resolved by a 10% SDS–polyacrylamide gel electrophoresis, and then transferred electrophoretically to a polyvinylidene difluoride membrane (Millipore, Billerica, MA). Membranes were incubated in 3% skimmed milk in a washing buffer, Tris-buffered saline containing 0.05% (v/v) Tween 20, for 2 h at room temperature. Then, membranes were incubated at 4°C overnight with an antinitrotyrosine mouse clone1A6 (Upstate Cell Signaling, Lake Placid, USA; 1 : 1000) or with goat anti β-actin primary antibody (Santa Cruz Biotechnology, Santa Cruz, CA; 1 : 100). After a wash, membranes were incubated with horseradish peroxidase-conjugated antimouse IgG (Sigma-Aldrich; 1 : 2000). Peroxidase activity was revealed by using enhanced chemiluminescence (ECL) reagent. Then, intensity of peroxidase activity was semiquantified using the ImageJ software. Results were corrected with the corresponding β-actin level and expressed as percentage of control group data.

For determination of GFAP, caspase-3 or caspase-9 expression, mice were decapitated 7 days after Aβ peptide injection. The hippocampi were removed on ice-cold glass plate and stored at −80°C. The hippocampus tissues were homogenized in ice-cold extraction buffer containing SDS 2% and proteases inhibitors (Roche). Equal amounts of protein, 40 µg per lane, were resolved by a 12% SDS–polyacrylamide gel electrophoresis, and then transferred electrophoretically to a nitrocellulose blot membrane (Schleicher Schuell 0.45 µm). The membranes were then blocked during 30 min at room temperature with 5% skim milk in Tris-buffered saline 20 mM (pH 7.6) containing 0.1% Tween 20 (TBS-T). The membranes were incubated at 4°C overnight with a mouse monoclonal anti-GFAP antibody (Sigma-Aldrich; 1 : 2000), or rabbit anticaspase-3 or rabbit anticaspase-9 antibody (Cell Signaling Technology; 1 : 1000 each), rinsed for 30 min in TBS-T and then incubated for 2 h with a goat antimouse or antirabbit secondary antibody (Sigma-Aldrich; 1 : 2000 each). Peroxidase activity was revealed by using ECL reagent. Then, intensity of peroxidase activity was semiquantified using the ImageJ software. Results were normalized to control values (anti β-tubulin; Sigma-Aldrich; 1 : 5000).

Statistical Analyses

Biochemical and behavioral data were expressed as mean ± SEM, except step-down latencies expressed as median and interquartile range. They were analyzed using one-way ANOVA (F-values), followed by the Dunnett's *post hoc* multiple comparison test. Passive avoidance latencies were analyzed a Kruskal–Wallis nonparametric ANOVA (H-values), as upper cutoff times were set, followed by the Dunn's multiple comparison test. The level of statistical significance was $p<0.05$.

RESULTS

Antiamnesic Effects of ANAVEX1-41 Against $A\beta_{25-35}$-Induced Learning Impairments

In the first series of experiments, the antiamnesic effects of ANAVEX1-41 was examined in mice centrally injected 7 days before with scrambled Aβ (ScAβ) or $A\beta_{25-35}$ peptide. The spatial working memory was first examined in the *Y*-maze test, animals receiving ANAVEX1-41 20 min before the session. As shown in Figure 1a, the central administration of ScAβ peptide or the subsequent i.p. treatment with ANAVEX1-41, in the 1–1000 µg/kg dose range, failed to change the spontaneous alternation performance that was in the 65–70% range ($F<1$). The treatments also did not affect the total number of arm entries ($F<1$; Figure 1b). When mice were treated with $A\beta_{25-35}$, the alternation performance decreased highly significantly to 53% and the ANAVEX1-41 treatment reversed the deficit ($F_{(8,145)}=4.41$, $p<0.0001$; Figure 1c). The compound showed a significant effect at the dose of 3 µg/kg and the improvement remained significant up to the highest dose tested. The most effective dose appeared to be 10 µg/kg. Neither the $A\beta_{25-35}$, nor the ANAVEX1-41 treatments affected the number of arm entries ($F_{(8,145)}=1.62$, $p>0.05$; Figure 1d).

The long-term contextual memory was evaluated using the step-down type passive avoidance procedure. Animals were tested 8 days after the central administration of ScAβ or $A\beta_{25-35}$ peptide and ANAVEX1-41 compound was administered 20 min before the first training session. The retention test was performed on day 9 after the peptide administration. As shown in Figure 2a and b, the ScAβ peptide or the subsequent treatment with ANAVEX1-41 in the 1–1000 µg/kg dose range, failed to affect the latency ($H=2.98$, $p>0.05$; Figure 2a) or percentage of animal-to-criterion that were in the 60–80% range (Figure 2b). In particular, the compound failed to show memory enhancing effect, as compared with V-treated animals. However, it must be noted that in procedures adapted to the measure of memory enhancing effects, the intensity of footshocks is lower than used in the present experiment. The central injection of $A\beta_{25-35}$ peptide led to highly significant decreases in latency ($H=27.72$, $p<0.001$; Figure 2c) and percentage of animals-to-criterion (Figure 2d). The ANAVEX1-41 treatment resulted in a bell shaped but highly significant reversion of the deficits. Both parameters revealed an active dose range of 1–100 µg/kg.

Neuroprotective Effects of ANAVEX1-41 Against the $A\beta_{25-35}$-Induced Learning Deficits

The neuroprotective effects of ANAVEX1-41 were first analyzed on the appearance of $A\beta_{25-35}$-induced learning deficits. The drug was administered in the same, 1–1000 µg/kg i.p., dose range and only once, 20 min before the i.c.v. administration of the peptide. We previously reported that such procedure is highly effective for mixed cholinergic/σ_1 compounds (Meunier *et al*, 2006). The pretreatment with ANAVEX1-41 resulted, 7 days after in a bell shaped but significant prevention of the $A\beta_{25-35}$-induced spontaneous alternation impairments ($F_{(8,145)}=3.40$, $p<0.01$; Figure 3a). The active doses of compound were in the 10–100 µg/kg

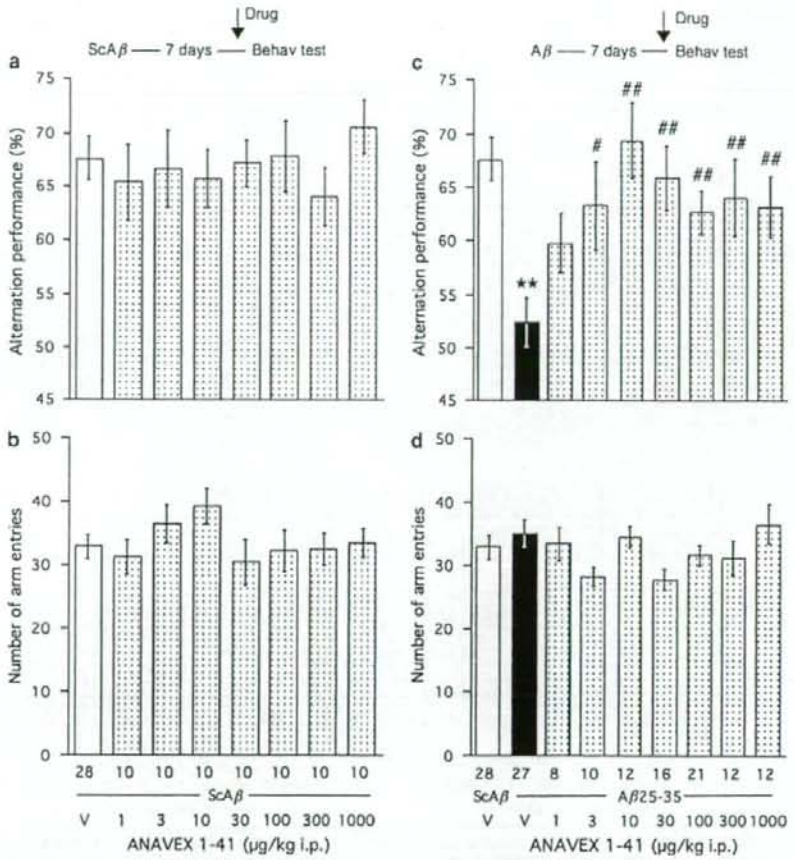

Figure 1 Antiamnesic effect of ANAVEX1-41 on $A\beta_{25-35}$-induced spontaneous alternation deficits in mice: alternation performances (a, c) and total numbers of arm entries (b, d). Mice were injected i.c.v. with ScAβ or $A\beta_{25-35}$ peptide (9 nmol). After 7 days, they were administered i.p. with the saline vehicle solution (V) or ANAVEX1-41 (1–1000 µg/kg), 30 min before being examined for spontaneous alternation in the Y-maze (see insert). The number of animals per group is indicated below the columns in (b) and (d). $^{**}p<0.01$ *vs* (ScAβ + V)-treated group; $^{\#}p<0.05$, $^{\#\#}p<0.01$ *vs* ($A\beta_{25-35}$ + V)-treated group; Dunnett's test.

range. No effect was observed in terms of number of arm entries ($F_{(8,145)}=1.64$, $p>0.05$; Figure 3b). The ANAVEX1-41 pretreatment also resulted in a significant prevention of the passive avoidance deficits, both in terms of latencies ($H=45.2$, $p<0.0001$; Figure 3c) and number of animals-to-criterion (Figure 3d). In this procedure, however, the active dose range was 30–300 µg/kg.

Neuroprotective Effects of ANAVEX1-41 Against $A\beta_{25-35}$-Induced Toxicity

Morphological validation of the protective effect of ANAVEX1-41 was examined using the most active dose of compound, 100 µg/kg. The pyramidal cell layer of the hippocampus is highly sensitive to the amyloid toxicity observed after $A\beta_{25-35}$ peptide injection in mice. We analyzed the number of viable cells in CA1 hippocampus area using cresyl violet staining (Figure 4). The $A\beta_{25-35}$ injection induced a −24.6% decrease in the number of viable cells in $A\beta_{25-35}$-treated mice ($F_{(3,20)}=7.68$, $p<0.01$; Figure 4c and e) as compared with ScAβ-treated mice (Figure 4a and e). In the same mice, no significant effect was measured in the CA3 area: 192 ± 6 cell per field ($n=6$) for the ScAβ group *vs* 187 ± 10 cell per field ($n=6$, $p>0.05$) for the $A\beta_{25-35}$ group. The ANAVEX1-41 treatment failed to affect the number of viable cells in the ScAβ-treated group (Figure 4b and e), but significantly attenuated the diminution observed after $A\beta_{25-35}$ treatment (Figure 4d and e).

The extent of brain inflammation after $A\beta_{25-35}$ and subsequent ANAVEX1-41 treatment was analyzed by measuring reactive astrocytes using GFAP immunohistolabeling (Figure 5). As the i.c.v. injection is expected to provoke by itself a massive glial reaction, ScAβ-treated groups were compared with animals receiving only the i.p. treatment with vehicle solution (Figure 5a, g, m and s) or ANAVEX1-41 (100 µg/kg; Figure 5b, h, n and t). Several

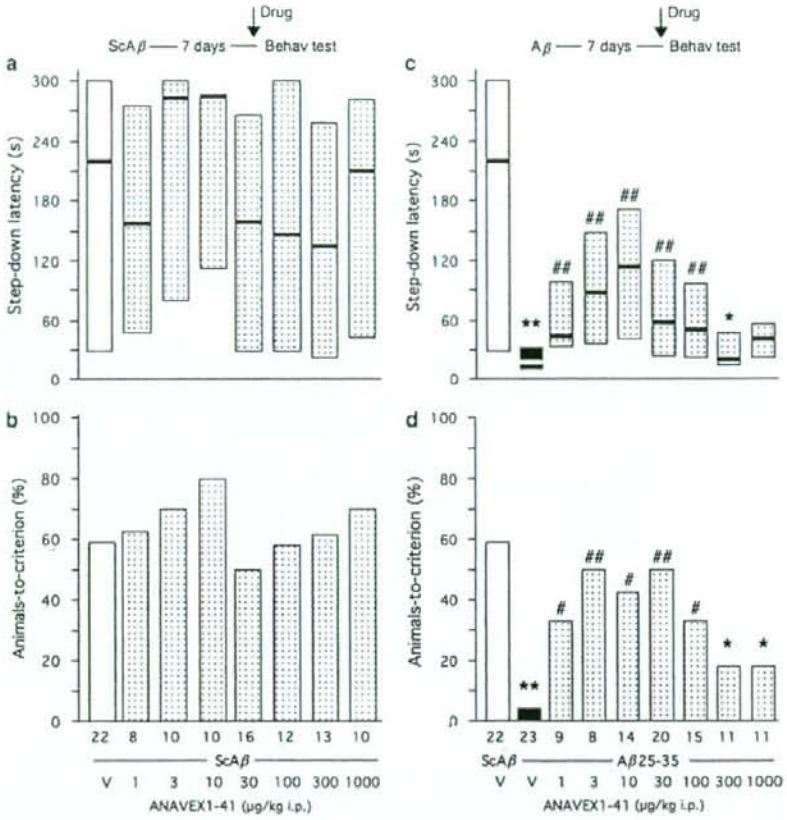

Figure 2 Effect of ANAVEX1-41 on $A\beta_{25-35}$-induced passive avoidance deficits in mice: step-down latency (a, c) and percentage of animals-to-criterion (b, d). Mice were injected i.c.v. with ScAβ or $A\beta_{25-35}$ peptide (9 nmol). After 7 days, they were administered i.p. with saline vehicle solution (V) or ANAVEX1-41 (1–1000 μg/kg), 30 min before the first training session (see insert). The number of animals is indicated below the columns in (b) and (d). $^{*}p<0.05$, $^{**}p<0.01$ *vs* (ScAβ + V)-treated group; $^{\#}p<0.05$, $^{\#\#}p<0.01$ *vs* ($A\beta_{25-35}$ + V)-treated group; Dunn's test in (a) and (c), χ^2-test in (b) and (d).

brain structures were analyzed and Figure 5 presents typical pictures in the retrosplenial (Figure 5a–f) and parietal (Figure 5g–l) cortices, where astrocytic clusters could be observed, and in the CA1 (Figure 5m–r) and CA3 (Figure 5s–x) areas of the hippocampus. In vehicle-treated animals, disseminated clusters containing few astrocytes were observed in the cortical areas (Figure 5a and g). The pattern of labeling was unchanged after ANAVEX1-41 i.p. injection and/or ScAβ i.c.v. injection (Figure 5b–d and h–j). $A\beta_{25-35}$ injection, however, provoked after 7 days a marked increase in the number of labeled astrocytes and in their branching, resulting in densification of astrocytic clusters. This was observed in the retrosplenial cortex (Figure 5e), but not in the parietal area (Figure 5k). The ANAVEX1-41 treatment resulted in a blockade of $A\beta_{25-35}$-induced increase of GFAP labeling (Figure 5f). In the hippocampus, astrocytes were regularly disseminated throughout the oriens and stratum radiatum layers surrounding the pyramidal cell layers (indicated by asterisks), at both the CA1 and CA3 levels (Figure 5m and s). These patterns were unchanged after ANAVEX1-41 i.p. injection and/or ScAβ i.c.v. injection (Figure 5n–p and t–v). The $A\beta_{25-35}$ injection, however, provoked a massive densification of astrocytic labeling both in CA1 (Figure 5q) and CA3 (Figure 5w). The ANAVEX1-41 treatment resulted in an attenuation of the $A\beta_{25-35}$-induced increase of GFAP labeling (Figure 5r and x).

Quantification of the increase in GFAP expression was performed in the hippocampus by western blotting. As shown in Figure 6, the ScAβ i.c.v. treatment or/and the ANAVEX1-41 i.p. treatment were without effect on GFAP expression. The $A\beta_{25-35}$ treatment significantly increased GFAP expression and this increase was blocked by ANAVEX1-41 ($F_{(5,49)}=5.59$, $p<0.001$; Figure 6). These data strengthened the qualitative immunohistochemical observations.

Several biochemical parameters of amyloid toxicity were also analyzed in the hippocampus extracts to validate the neuroprotective activity of ANAVEX1-41. First, amyloid peptides, and particularly $A\beta_{25-35}$, induce a massive oxidative stress in forebrain structures. We therefore analyzed in the levels of lipid peroxidation (Figure 7a) and protein nitration (Figure 7b) and induction of caspase-9 expression, a marker of mitochondrial damage (Figure 7c).

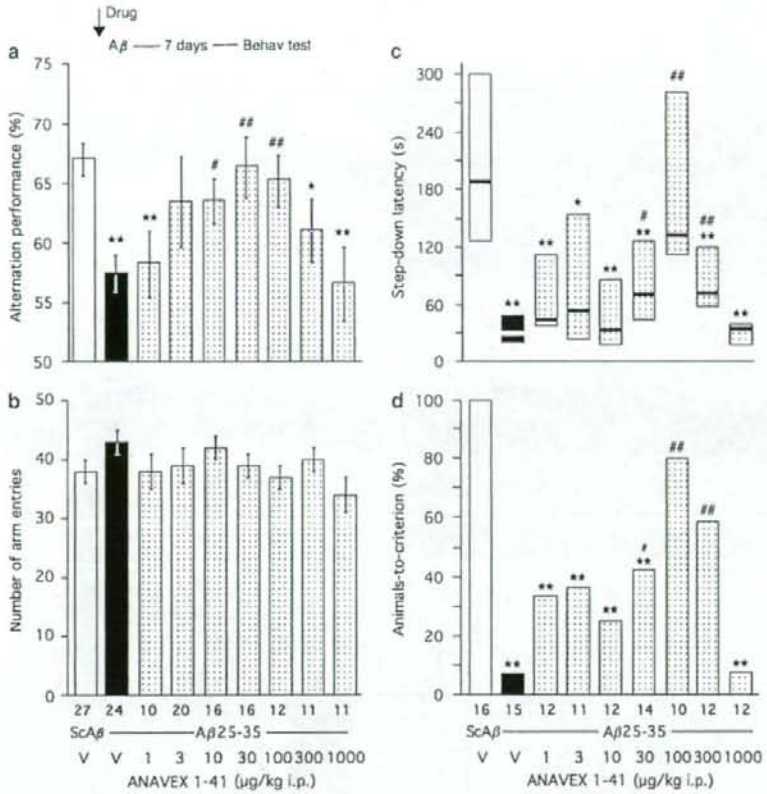

Figure 3 Neuroprotective effect of ANAVEX1-41 on $A\beta_{25-35}$-induced learning deficits in mice: alternation performance (a) and number of arm entries (b) in the Y-maze test; step-down latency (c) and percentage of animals-to-criterion (d) in the passive avoidance test. Mice were administered i.p. with vehicle solution (saline, V) or ANAVEX1-41 (1–1000 μg/kg) 20 min before being injected i.c.v. with ScAβ or $A\beta_{25-35}$ peptide (9 nmol). After 7 days, they were examined for spontaneous alternation or trained in the passive avoidance test (see insert). The number of animals per group is indicated below the columns in (b) and (d). $^{*}p<0.05$, $^{**}p<0.01$ *vs* (ScAβ + V)-treated group; $^{\#}p<0.05$, $^{\#\#}p<0.01$ *vs* ($A\beta_{25-35}$ + V)-treated group; Dunnett's test in (a), Dunn's test in (c), χ^2-test in (d).

Second, amyloid toxicity results in cell death through caspase-dependent apoptosis pathways. We therefore measured the induction of caspase-3 expression (Figure 7d).

$A\beta_{25-35}$ induced a +117% increase in the level of peroxidized lipids that could be measured in the hippocampus ($F_{(6,82)}=8.07$, $p<0.0001$; Figure 7a). ANAVEX1-41, tested in the 10–1000 μg/kg i.p. dose range, highly significantly, but in a U-shaped manner, prevented the $A\beta_{25-35}$-induced increase in lipid peroxidation. The protective effect was measured at 30 and 100 μg/kg (Figure 7a). The western blot analysis of protein nitration revealed only a single band for nitrated proteins at the size of 70 kDa (Figure 7b, see Supplementary Figure 1 for the whole blot). $A\beta_{25-35}$ induced a +30% increase in nitrotyrosine immunoreactivity ($F_{(3,23)}=8.99$, $p<0.001$; Figure 7b). The pretreatment with ANAVEX1-41, 100 μg/kg i.p., tended to decrease the level of nitrotyrosine immunoreactivity in ScAβ-treated mice (−19%, $p>0.05$) but highly significantly prevented the $A\beta_{25-35}$-induced increase (Figure 7b). The western blot analysis of caspase-9 expression revealed only a single band at the size of 49 kDa that corresponded to procaspase-9 (Figure 7c). $A\beta_{25-35}$ induced a +38% increase in caspase-9 expression ($F_{(3,51)}=4.13$, $p<0.05$; Figure 7c). The pretreatment with ANAVEX1-41, 100 μg/kg i.p., failed to affect caspase-9 expression in ScAβ- or $A\beta_{25-35}$-treated animals (Figure 7c). The western blot analysis of caspase-3 expression revealed only a single band at the size of 35 kDa that corresponded to the cleaved form of caspase-3 (Figure 7d). $A\beta_{25-35}$ induced a +32% increase in caspase-3 induction ($F_{(3,34)}=4.31$, $p<0.05$; Figure 7d). The pretreatment with ANAVEX1-41, 100 μg/kg i.p., significantly prevented the $A\beta_{25-35}$-induced increase (Figure 7d). However, the treatment also resulted in a significant increase in the level of caspase-3 induction in ScAβ-treated mice (+20%, $p<0.05$; Figure 7d).

Involvement of (i) Muscarinic receptors and (ii) σ_1 Protein in the Neuroprotective Effect of ANAVEX1-41

The compound is equally active, with binding affinities in the 18–114 nM range, on muscarinic M_1–M_4 receptors and the σ_1 protein (Espallergues *et al*, 2007). To determine

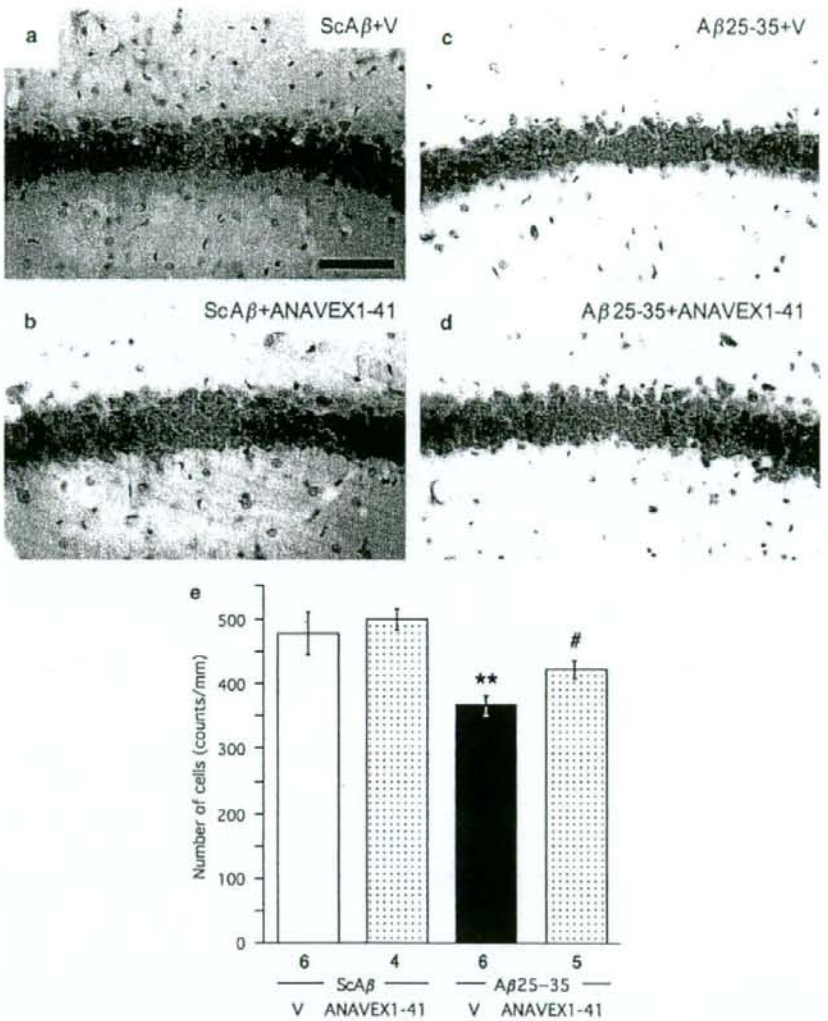

Figure 4 Neuroprotective effect of ANAVEX1-41 on $A\beta_{25-35}$-induced toxicity in mice: pyramidal cell loss in the CA1 area of the hippocampal pyramidal cell layer, 7 days after $A\beta_{25-35}$ injection. (a–d) Representative microphotographs of coronal sections of cresyl violet stained hippocampal CA1 subfield. (e) Averaged levels of viable cells. Mice were administered i.p. with saline vehicle solution (V) or ANAVEX1-41 (100 μg/kg), 20 min before being administered i.c.v. with $A\beta_{25-35}$ peptide (9 nmol). Scale bar shown in (a) = 100 μm. At least six slices were counted per mice and the number of mice used per group is indicated below the columns in (e). $^{**}p<0.01$ *vs* (ScAβ + V)-treated group; $^{\#}p<0.05$ *vs* ($A\beta_{25-35}$ + V)-treated group; Dunnett's test.

whether both pharmacological targets are involved in the protective effects of the compound, we coadministered: (i) the muscarinic receptor antagonist scopolamine (0.5 mg/kg) or (ii) the σ_1 protein inactivator BD1047 (1 mg/kg) with the active doses of ANAVEX1-41 (30, 100 μg/kg). The learning abilities were analyzed after 7 days using the *Y*-maze and passive avoidance procedures. As shown in Figure 8a, the muscarinic receptor antagonist attenuated the ANAVEX1-41 effect, nonsignificantly against the 30 μg/kg dose of ANAVEX1-41 and significantly against 100 μg/kg ($F_{(6,119)}=5.14$, $p=0.0001$). The BD1047 treatment led to a similar effect (Figure 8b). BD1047 attenuated the ANAVEX1-41 effect, nonsignificantly against the 30 μg/kg dose of ANAVEX1-41 and significantly against 100 μg/kg ($F_{(6,114)}=4.55$, $p<0.001$; Figure 8b). In the passive avoidance test, scopolamine pretreatment also fully prevented the ANAVEX1-41 (100 μg/kg) effect, but not the ANAVEX1-41 (30 μg/kg) effect, similarly for latency ($H=30.6$, $p<0.0001$; Figure 9a) and animals-to-criterion (Figure 9b). However, different results were obtained in the contextual memory procedure with BD1047. The σ_1 protein inactivator significantly blocked the beneficial effect of 30 μg/kg